Reduced-Rank Multistage Receivers for DS-CDMA in Frequency-Selective Fading Channels

Sau-Hsuan Wu, *Member, IEEE*, Urbashi Mitra, *Senior Member, IEEE*, and C.-C. Jay Kuo, *Fellow, IEEE*

***Abstract*—Multistage (MS) implementation of the minimum mean-square error (MMSE), minimum output energy (MOE), best linear unbiased estimation (BLUE), and maximum-likelihood (ML) filter banks (FBs) is developed based on the concept of the MS Wiener filtering (MSWF) introduced by Goldstein *et al.* These FBs are shown to share a common MS structure for interference suppression, modulo a distinctive scaling matrix at each filter's output. Based on this finding, a framework is proposed for joint channel estimation and multiuser detection (MUD) in frequency-selective fading channels. Adaptive reduced-rank equal gain combining (EGC) schemes for this family of FBs (MMSE, MOE, BLUE, and ML) are proposed for noncoherent blind MUD of direct-sequence code-division multiple-access systems, and contrasted with the maximal ratio combining counterparts that are also formed with the proposed common structure under the assumption of known channel-state information. The bit-error rate, steady-state output signal-to-interference plus noise ratio (SINR), and convergence of the output SINRs are investigated via computer simulation. Simulation results indicate that the output SINRs attain full-rank performance with much lower rank for a highly loaded system, and that the adaptive reduced-rank EGC BLUE/ML FBs outperform the EGC MMSE/MOE FBs, due to the unbiased nature of the implicit BLUE channel estimators employed in the EGC BLUE/ML schemes.**

***Index Terms*—Best linear unbiased estimation (BLUE), code-division multiple access (CDMA), maximum-likelihood (ML), minimum mean-square error (MMSE), minimum output energy (MOE), multipath fading channels, multistage Wiener filtering (MSWF), multiuser detection (MUD), reduced-rank filtering, time-varying channels.**

I. Introduction

REDUCED-RANK linear filtering based on the multistage Wiener filter (MSWF) of [1] has proven to be an effective detection scheme for multiuser direct-sequence code-division multiple-access (DS-CDMA) systems in additive white Gaussian noise (AWGN) channels [2]. A class of adaptive reduced-rank schemes of MSWF was provided [2], and shown to achieve near full-rank performance with relatively fewer dimensions, in comparison with reduced-rank schemes based on eigen-decomposition methods (e.g., [3]). Thus, the number of samples required for adaptive implementation is greatly reduced, and better tracking performance can be obtained in time-varying systems and channel conditions. Moreover, the MSWF does not require an explicit estimate of the signal subspace, which makes it more robust to estimation uncertainties.

Paper approved by J. Wang, the Editor for Wireless Spread Spectrum of the IEEE Communications Society. Manuscript received April 29, 2003; revised June 10, 2004. This work was supported in part by the Integrated Media Systems Center, a National Science Foundation Engineering Research Center, under Cooperative Agreement EEC-9529152, and in part by the National Science Foundation under Grant NSF/ANI-0087761.

The authors are with the Department of Electrical Engineering, University of Southern California, Los Angeles, CA 90089-2564 USA (e-mail: sauhsuaw@costard.usc.edu; ubli@usc.edu; ckuo@sipi.usc.edu)

Digital Object Identifier 10.1109/TCOMM.2004.842003

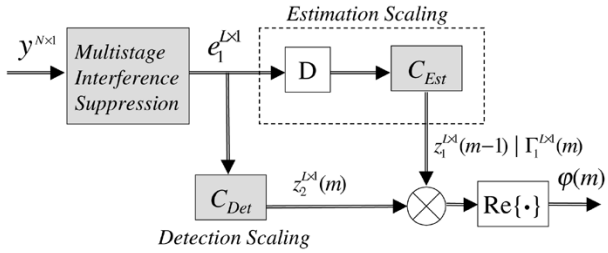

Fig. 1. Framework for joint channel estimation and MUD in multipath fading channels. For MRC receivers, the estimation scaling part is not necessary, and $\mathbf{z}_1(m-1)$ is replaced by the given channel vector $\Gamma_1(m)$. For EGC receivers, the matrices $C_{\rm Est}$ and $C_{\rm Det}$ can be any of the scaling matrices of the MMSE/MOE/BLUE/ML FBs.

To exploit the diversity offered by a multipath fading channel, maximal ratio combining (MRC) is often employed to achieve the maximal signal-to-noise ratio (SNR), given channel state information (CSI). In the absence of CSI, it was suggested in [4] and [5] to adopt an adaptive multiple minimum mean-square error (MMSE)/ minimum output energy (MOE) filter structure for interference suppression along each resolvable transmission path of the desired user. Filter outputs along each resolvable path are first differentially decoded, and then results from each path are linearly combined with an equal gain to form decision statistics. Detection schemes of this kind are referred to as noncoherent equal-gain combining (EGC) receivers [4]. However, for reduced-rank detection, receivers which jointly suppress interference in a multipath fading channel outperform those that suppress interference path by path [6]. Based on these arguments and the concept of MSWF [1], we develop herein multistage (MS) implementation of the MMSE, MOE, best linear unbiased estimation (BLUE), and maximum-likelihood (ML) filter banks (FBs) for interference suppression in multipath fading channels. These FBs are shown to share a common MS structure for interference suppression, modulo a distinctive scaling matrix at each filter's output. With this common structure, a framework is proposed for joint channel estimation and multiuser detection (MUD) in fast-fading channels, as shown in Fig. 1, whereby various combining schemes, e.g., BLUE-ML and BLUE-MMSE combinings, can be efficiently implemented and evaluated without extra implementation complexity.

For reduced-rank filters, the dimension of subspaces required for achieving satisfactory output signal-to-interference plus noise ratios (SINRs) is an important measure. With the same output SINR, lower rank implies faster convergence, and thus,

potentially better performance in dynamic environments. The output SINRs of the MS FBs developed herein are investigated through a recursive adaptation scheme generalized from [2] for MSWF. Performance comparisons of the MMSE, MOE, BLUE, and ML FBs are conducted for coherent MRC and noncoherent EGC via simulations in the context of MUD of DS-CDMA in multipath Rayleigh fading channels. Based on these results, a new type of EGC ML detection scheme is proposed, which accrues the advantages of both unbiased channel estimation and reduced-rank MUD.

The rest of this paper is organized as follows. Section II describes the system model for asynchronous DS-CDMA in multipath fading channels. The MS MMSE/MOE receivers for multipath fading channels are derived in Section III. Extensions to the MS BLUE/ML receivers are made in Section IV, followed by the exposition of the common structure for reduced-rank MUD in Section V. The structural differences between the MS pre- and post-combining interference suppression are detailed in Section VI. The numerical simulation results are presented in Section VII, and concluding remarks are drawn in Section VIII.

II. System Model

A standard model for asynchronous DS-CDMA is considered. The baseband representation of the transmitted signal for the kth user can be written as

$$x_k(t) = \sqrt{2P_k} \sum_{n=-\infty}^{\infty} b_k(n) s_k(t - nT_s - \tau_k) \qquad (1)$$

where T_s is the symbol duration, and $b_k(n)$, P_k, and τ_k are the data bit at time n, energy per bit, and relative delay with reference to the base station, respectively, for the kth user. The transmitted symbols, $b_k(n)$, are identically and independently distributed (i.i.d.), taking on the values $\{-1, 1\}$ with equal probabilities. The spreading waveform is given by $s_k(t) = \sum_{i=0}^{N-1} c_k(j)\psi(t - jT_c)$, where $c_k(i) \in \left\{(-1/\sqrt{N}), (1/\sqrt{N})\right\}$ is the signature sequence for the kth user with a period of N. The function $\psi(t)$ is a normalized chip pulse-shaping function of duration T_c, with $T_s/T_c = N$ being the spreading gain.

The kth user's signal $x_k(t)$ propagates through a multipath fading channel with the complex impulse response $g_k(t) = \sum_{l=1}^{L_k} g_{kl}(t)\delta_D(t - \eta_{kl})$, where $\delta_D(t)$ is the Dirac delta function, L_k is the number of the paths for user k, η_{kl} is the delay time associated with the lth tap of the tapped-delay-line channel model, and $g_{kl}(t)$ is the fading process corresponding to the tap. The value of $g_{kl}(t)$ is assumed to be constant during one symbol interval, and changes from symbol to symbol. Thus, $g_{kl}(t)$ can be modeled by a discrete-time fading process $a_{kl}\gamma_{kl}(m)$, where a_{kl} is a time-invariant nonnegative channel gain, and $\gamma_{kl}(m)$ is a complex zero-mean Gaussian process satisfying $E[\gamma^*_{k_1 l_1}(m)\gamma_{k_2 l_2}(m)] = \delta_K(k_1 - k_2)\delta_K(l_1 - l_2)$ (here δ_K denotes the Kronecker delta function), and the autocorrelation value of two adjacent channel samples is $\rho \triangleq E[\gamma^*_{k_1 l_1}(m)\gamma_{k_1 l_1}(m-1)]$, $0 \le \rho < 1, \forall\, m$. Convolving the transmitted signal with the channel impulse response, the received signal due to the kth user is given by

$$\begin{aligned} r_k(t) &= x_k(t) * g_k(t) \\ &= \sqrt{2P_k} \sum_{n=-\infty}^{\infty} b_k(n) \sum_{j=0}^{N-1} \sum_{l=1}^{L_k} g_{kl}(t) c_k(j) \\ &\quad \times \psi(t - nT_s - jT_c - \tau_{kl}) \end{aligned} \qquad (2)$$

where $\tau_{kl} \triangleq \tau_k + \eta_{kl}$. The overall received signal is given by $r(t) = \sum_{k=1}^{K} r_k(t) + n(t)$, where K is the number of users, and $n(t)$ is complex zero-mean white Gaussian noise.

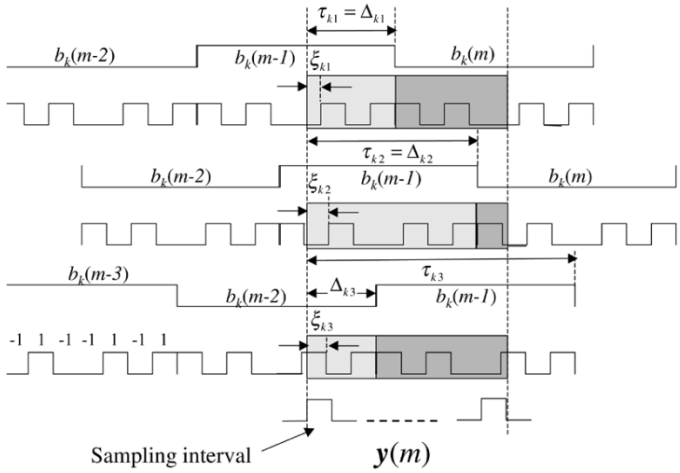

Fig. 2. Delay pattern of a three-path DS-CDMA channel of user k. The light-shaded regions belong to the symbols that arrive earlier inside the sampling interval of $\mathbf{y}(m)$, compared with the dark-shaded regions, which belong to the symbols that arrive later in the same transmission paths of the same sampling interval.

To demonstrate the main ideas of our proposed schemes, we consider one-shot detection, and assume that the maximum delay spread $|\max_l\{\tau_{kl}\} - \min_l\{\tau_{kl}\}| < T_s$ for all users. Thus, the delay $\tau_{k1} < T_s$ for the first path of every user, and $\tau_{kl} < 2T_s$, $l \ge 2$. For cases where delay spreads are larger than T_s, the detection windows can be simply extended for more than one symbol duration to capture the signal belonging to the longest delay path among all users. Without loss of generality, user 1 is chosen to be the desired user. It is assumed that the delay time for each path of the desired user is known, and it is further assumed that the receiver's clock is synchronized with the reception of the first path of the desired user, i.e., $\tau_{11} = 0$ and $\tau_{1l} < T_s$, $l \ge 2$. We define $m_{kl} \triangleq \lfloor \tau_{kl}/T_s \rfloor$, $m_{kl} \in \{0, 1\}$, where $\lfloor \cdot \rfloor$ denotes the largest integer less than or equal to the argument, $\Delta_{kl} \triangleq T_s | \tau_{kl}$, $i_{kl} \triangleq \lfloor \Delta_{kl}/T_c \rfloor$, $0 \le i_{kl} < N - 1$, and $\xi_{kl} T_c \triangleq T_c | \Delta_{kl}$, $0 \le \xi_{kl} < 1$, where $a \mid b$ denotes the remainder of b divided by a. An example of a three-path delay pattern for user k is illustrated in Fig. 2.

The received signal is passed through a filter matched to the chip pulse-shaping function $\psi(t - mT_s - iT_c)$, and then sampled at the chip rate. We define $\mathbf{c}_k^L(i_{kl}) \triangleq [0 \ldots 0, c_k(0) \ldots c_k(N - i_{kl} - 1)]^T$ and $\mathbf{c}_k^R(i_{kl}) \triangleq [c_k(N - i_{kl}) \ldots c_k(N-1), 0 \ldots 0]^T$; both vectors are of dimension $N \times 1$. Due to the asynchronous arrival times, the contribution of the signature sequence due to the earlier arrival symbol for path l in Fig. 2 can be expressed as $\mathbf{s}_{kl}^- \triangleq (1 - \xi_{kl})\mathbf{c}_k^R(i_{kl}) + \xi_{kl}\mathbf{c}_k^R(i_{kl} + 1)$, and the contribution

of the signature sequence due to the later arrival symbol on path l is equal to $\mathbf{s}_{kl}^{+} \triangleq (1-\xi_{kl})\mathbf{c}_k^L(i_{kl}) + \xi_{kl}\mathbf{c}_k^L(i_{kl}+1)$. Thus, the discrete-time signal vector $\mathbf{y}$ obtained by collecting N consecutive samples of the matched-filter output is given by (e.g., [4])

$$\mathbf{y}(m) = \sum_{k=1}^{K}\sum_{l=1}^{L_k} A_{kl}\gamma_{kl}(m)\left[\mathbf{s}_{kl}^{+}b_k(m-m_{kl}) + \mathbf{s}_{kl}^{-}b_k(m-m_{kl}-1)\right] + \mathbf{n}(m) \quad (3)$$

where $A_{kl} \triangleq a_{kl}\sqrt{2P_k}$. The filtered noise vector $\mathbf{n}(m)$ is complex Gaussian distributed with covariance matrix $N_0\mathbf{I}$. Note that $m_{1l} = 0$. For convenience of analysis, the discrete-time received signal $\mathbf{y}(m)$ can be rewritten as

$$\begin{aligned}\mathbf{y}(m) = {} & \mathbf{S}_{1+}\mathbf{A}_1\Gamma_1(m)b_1(m) + \mathbf{S}_{1-}\mathbf{A}_1\Gamma_1(m)b_1(m-1) \\ & + \sum_{k=2}^{K}\sum_{l=1}^{L_k} A_{kl}\gamma_{kl}(m) \\ & \times \left[\mathbf{s}_{kl}^{+}b_k(m-m_{kl}) + \mathbf{s}_{kl}^{-}b_k(m-m_{kl}-1)\right] + \mathbf{n}(m)\end{aligned} \quad (4)$$

where $\mathbf{A}_1 \triangleq \mathrm{diag}([A_{11},\ldots,A_{1L_1}])$, $\mathbf{S}_{1+} \triangleq \left[\mathbf{s}_{11}^{+},\ldots,\mathbf{s}_{1L_1}^{+}\right]$, $\mathbf{S}_{1-} \triangleq \left[\mathbf{s}_{11}^{-},\ldots,\mathbf{s}_{1L_1}^{-}\right]$, and $\Gamma_1 \triangleq [\gamma_{11},\ldots,\gamma_{1L_1}]^T$. The matrix $\mathbf{S}_{1+}$ is referred to as the steering matrix for the desired user's signal.

Note that in this paper, a boldface capital letter $\mathbf{X}^{p\times q}$ denotes a matrix of dimension p by q, and a boldface lowercase letter $\mathbf{x}^{p\times 1}$ denotes a vector of dimension $p\times 1$. The Hermitian of a matrix or vector is denoted by $\mathbf{X}^H$ or $\mathbf{x}^H$, and the transpose of a matrix or vector is denoted by $\mathbf{X}^T$ or $\mathbf{x}^T$. For convenience of presentation, the time index m of a variable is suppressed if not necessary, and $L \equiv L_1$ in the remainder of this paper.

III. MS MMSE-Based FBs

Before we introduce the MS implementation of the MMSE and MOE FBs, we first briefly review the MMSE reception of DS-CDMA and its limitations in fast-fading channels. The concept of the MSWF is later introduced to motivate the succeeding derivations for the MS MMSE/MOE FBs.

The MMSE receiver for DS-CDMA systems is given by (see, e.g., [7])

$$\begin{aligned}\hat{\boldsymbol{\omega}} &= \arg\min_{\omega} E\left\|b_1 - \omega^H\mathbf{y}\right\|^2 \\ &= \mathbf{R}^{-1}E(\mathbf{y}b_1^*) = \mathbf{R}^{-1}\mathbf{S}_{1+}\mathbf{A}_1E(\Gamma_1)\end{aligned} \quad (5)$$

where $\mathbf{R} = E(\mathbf{y}\mathbf{y}^H)$. In fast-fading channels, $E(\Gamma_1) = \mathbf{0}$, and the MMSE receiver in (5) degenerates to the zero vector. A modified MMSE filter, in conjunction with the use of differential encoding, was proposed in [4] to exploit the multipath diversity without the desired user's channel information. The cost function in (5) is modified to the form of

$$\omega_{\mathrm{mmse}} = \arg\min_{\omega} E\left\|b_1\Gamma_1 - \omega^H\mathbf{y}\right\|^2 = \mathbf{R}^{-1}\mathbf{S}_{1+}\mathbf{A}_1\boldsymbol{\Sigma}_1 \quad (6)$$

where the objective of estimation becomes the product of the channel and the data, and $\boldsymbol{\Sigma}_1 \triangleq \mathrm{Cov}(\Gamma_1) = \mathbf{I}$, by definition in the previous section. The filter's soft-output vector, $\mathbf{z}(m)$, of dimension $L\times 1$ and the detection method for differential BPSK (DBPSK) are given by

$$\mathbf{z}(m) = \omega_{\mathrm{mmse}}^H\mathbf{y}(m) \quad (7)$$

$$\begin{aligned}\hat{b_1}(m) &= \mathrm{sgn}\{\Re[\mathbf{z}^H(m)\mathbf{z}(m-1)]\} \\ &\triangleq \mathrm{sgn}\{\Re[\varphi(m)]\}\end{aligned} \quad (8)$$

where φ is the decision statistic for b_1. This type of reception is referred to as differential EGC of the MMSE FB (EGC-MMSE-FB) [4]. With the same argument, the MOE filter for AWGN channels in [8] is also modified in [4] for differential detection in multipath channels, with the criterion given by

$$\begin{aligned}\omega_{\mathrm{moe}} &= \arg\min_{\omega} E\|\omega^H\mathbf{y}\|^2 \\ \text{subject to } \omega_{\mathrm{moe}}^H\mathbf{S}_{1+}\mathbf{A}_1 &= \mathbf{A}_1\mathbf{S}_{1+}^H\mathbf{S}_{1+}\mathbf{A}_1.\end{aligned} \quad (9)$$

The solution can be shown equal to

$$\omega_{\mathrm{moe}} = \mathbf{R}^{-1}\mathbf{S}_{1+}\left(\mathbf{S}_{1+}^H\mathbf{R}^{-1}\mathbf{S}_{1+}\right)^{-1}\mathbf{S}_{1+}^H\mathbf{S}_{1+}\mathbf{A}_1. \quad (10)$$

The corresponding detection method, (8), is referred to as differential EGC of the MOE FB (EGC-MOE-FB) [4].

To motivate the derivations for the MMSE/MOE FBs, we next briefly review the key idea of MSWF. It is shown in [1] that the mean-squared error (MSE) of an MMSE filter is invariant to an unitary transform $\mathbf{T}$ applied to the signal $\mathbf{y}$, i.e.,

$$\min_{\boldsymbol{\omega}} E\left\|b_1 - \omega^H\mathbf{y}\right\|^2 = \min_{\boldsymbol{\omega}} E\left\|b_1 - \omega^H\mathbf{T}\mathbf{y}\right\|^2. \quad (11)$$

If the matrix $\mathbf{T}$ is chosen to be $\mathbf{T}^H \triangleq \left[\mathbf{h}_1 \mid \mathbf{B}_1^H\right]$, where $\mathbf{h}_1 \triangleq E(\mathbf{y}b_1^*)/\|E(\mathbf{y}b_1^*)\|^2$ and $\mathbf{B}_1\mathbf{h}_1 = \mathbf{0}$, denoted by $\mathbf{h}_1 \perp \mathbf{B}_1^H$, the MMSE filter in (5) can be decomposed into a linear combination of a matched filter and another MMSE filter. Successively applying the idea of (11) to every resultant MMSE filter, the MMSE filter in (5) can finally be decomposed to a structure of MS matched filters, and is thus referred to as the MSWF. The MSWF was later applied to DS-CDMA in AWGN channels in [2] for reduced-rank MUD. Our objective herein is to extend the notion of the MSWF to a host of blind MUD schemes for DS-CDMA signaling in multipath fading channels.

A. MS MMSE FB

We next generalize the method in [1] to estimate the vector $b_1\Gamma_1$. Assuming that the steering matrix $\mathbf{S}_{1+}^{N\times L}$ is of full column rank, it can be decomposed via the Gram–Schmidt process as

$$\mathbf{S}_{1+} = \mathbf{H}_1^{N\times L}\mathbf{U}_1^{L\times L} \quad (12)$$

where the column vectors of $\mathbf{H}_1$ form an orthonormal basis, i.e., $\mathbf{H}_1^H\mathbf{H}_1 = \mathbf{I}$, that spans the column space of $\mathbf{S}_{1+}$. We denote the subspace spanned by the column vectors of $\mathbf{H}_1$ by $\mathcal{H}_1$, and refer to it as the *signal subspace*. Next, we form a unitary matrix $\mathbf{T}^{N\times N}$ of the form

$$\mathbf{T}^H \triangleq \left[\mathbf{H}_1 \mid \mathbf{B}_1^H\right] \quad (13)$$

where $\mathbf{B}_1^{(N-L)\times N}\mathbf{H}_1^{N\times L} = \mathbf{0}$, denoted by $\mathbf{B}_1^H \perp \mathbf{H}_1$. The matrix $\mathbf{B}_1$ is often referred to as the *blocking matrix* of $\mathbf{S}_{1+}$, and

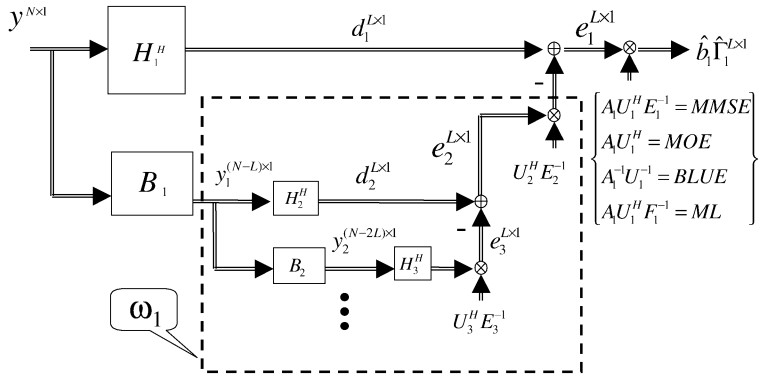

Fig. 3. Structure of the MS MMSE/MOE/BLUE/ML FBs for channel estimation and MUD in multipath fading channels. The output scaling matrix is $\mathbf{A}_1\mathbf{U}_1^H\mathbf{E}_1^{-1}$ for the MS-MMSE-FB, $\mathbf{A}_1\mathbf{U}_1^H$ for the MS-MOE-FB, $\mathbf{A}_1^{-1}\mathbf{U}_1^{-1}$ for the MS-BLUE-FB, and $\mathbf{A}_1\mathbf{U}_1^H\mathbf{F}_1^{-1}$ for the MS-ML-FB. The objective of estimation is $b_1\Gamma_1$.

can be obtained via the QR factorization of $\mathbf{S}_{1+}$. We now invoke the invariance of the MSE to a unitary transform, i.e.,

$$\min_{\omega} E\left\|b_1\Gamma_1-\omega^H\mathbf{y}\right\|^2=\min_{\omega} E\left\|b_1\Gamma_1-\omega^H\mathbf{T}\mathbf{y}\right\|^2. \quad (14)$$

The solution to (14) is given by

$$\begin{aligned}\omega_{\mathrm{mmse}}^{N\times L}&=\arg\min_{\omega} E\left\|b_1\Gamma_1-\omega^H\mathbf{T}\mathbf{y}\right\|^2\\&=(\mathbf{T}\mathbf{R}\mathbf{T}^H)^{-1}\mathbf{T}\mathbf{S}_{1+}\mathbf{A}_1. \end{aligned}\quad (15)$$

The invariance of the MSE can be easily verified, due to the fact that $\mathbf{A}_1\mathbf{S}_{1+}^H\mathbf{T}^H(\mathbf{T}\mathbf{R}\mathbf{T}^H)^{-1}\mathbf{T}\mathbf{y}=\mathbf{A}_1\mathbf{S}_{1+}^H\mathbf{R}^{-1}\mathbf{y}$, since $\mathbf{T}^H=\mathbf{T}^{-1}$. The application of $\mathbf{T}$ separates the signal component of $\mathbf{y}$ lying in the subspace $\mathcal{H}_1$ from the component lying in $\mathcal{H}_1$'s orthogonal complement, $\mathcal{B}_1$, which is spanned by the column vectors of $\mathbf{B}_1^H$. The projected vector $\mathbf{B}_1\mathbf{y}$ is used to suppress the projected multiple-access interference (MAI) in the signal subspace $\mathcal{H}_1$. This concept will be discussed more rigorously in Section III-C, following the derivation of the MS-MOE-FB.

Substituting (13) into (15) and applying the matrix-inversion lemma [9] to $(\mathbf{T}\mathbf{R}\mathbf{T}^H)^{-1}$, the MMSE FB ω_{mmse} becomes

$$\begin{aligned}\omega_{\mathrm{mmse}}&=\left(\left[\frac{\mathbf{H}_1^H}{\mathbf{B}_1}\right]\mathbf{R}\left[\mathbf{H}_1\;\middle|\;\mathbf{B}_1^H\right]\right)^{-1}\left[\frac{\mathbf{H}_1^H}{\mathbf{B}_1}\right]\mathbf{S}_{1+}\mathbf{A}_1\\&=\left(E\left[\frac{\mathbf{d}_1\mathbf{d}_1^H\;\middle|\;\mathbf{d}_1\mathbf{y}_1^H}{\mathbf{y}_1\mathbf{d}_1^H\;\middle|\;\mathbf{y}_1\mathbf{y}_1^H}\right]\right)^{-1}\left[\frac{\mathbf{U}_1}{\mathbf{0}}\right]\mathbf{A}_1\\&\triangleq\left[\frac{\mathbf{R}_{\mathbf{d}_1}\;\middle|\;\boldsymbol{\Upsilon}_{\mathbf{y}_1\mathbf{d}_1}^H}{\boldsymbol{\Upsilon}_{\mathbf{y}_1\mathbf{d}_1}\;\middle|\;\mathbf{R}_{\mathbf{y}_1}}\right]^{-1}\left[\frac{\mathbf{U}_1}{\mathbf{0}}\right]\mathbf{A}_1\\&=\left[\frac{\mathbf{E}_1^{-1}\;\middle|\;-\mathbf{E}_1^{-1}\boldsymbol{\Upsilon}_{\mathbf{y}_1\mathbf{d}_1}^H\mathbf{R}_{\mathbf{y}_1}^{-1}}{-\mathbf{R}_{\mathbf{y}_1}^{-1}\boldsymbol{\Upsilon}_{\mathbf{y}_1\mathbf{d}_1}\mathbf{E}_1^{-1}\;\middle|\;\Delta}\right]\\&\quad\times\left[\frac{\mathbf{U}_1}{\mathbf{0}}\right]\mathbf{A}_1\\&=\left[\frac{\mathbf{I}}{-\mathbf{R}_{\mathbf{y}_1}^{-1}\boldsymbol{\Upsilon}_{\mathbf{y}_1\mathbf{d}_1}}\right]\mathbf{E}_1^{-1}\mathbf{U}_1\mathbf{A}_1\end{aligned}\quad (16)$$

where $\mathbf{d}_1^{L\times 1}\triangleq\mathbf{H}_1^H\mathbf{y}$ and $\mathbf{y}_1^{(N-L)\times 1}\triangleq\mathbf{B}_1\mathbf{y}$; $\mathbf{R}_{\mathbf{d}_1}$ and $\mathbf{R}_{\mathbf{y}_1}$ are the autocorrelation matrices of $\mathbf{d}_1$ and $\mathbf{y}_1$, respectively; and $\boldsymbol{\Upsilon}_{\mathbf{y}_1\mathbf{d}_1}\triangleq E\left(\mathbf{y}_1\mathbf{d}_1^H\right)$ is the crosscorrelation matrix of $\mathbf{y}_1$ and $\mathbf{d}_1$. The matrix $\mathbf{E}_1\triangleq\left(\mathbf{R}_{\mathbf{d}_1}-\boldsymbol{\Upsilon}_{\mathbf{y}_1\mathbf{d}_1}^H\mathbf{R}_{\mathbf{y}_1}^{-1}\boldsymbol{\Upsilon}_{\mathbf{y}_1\mathbf{d}_1}\right)$, and the matrix Δ is not specified, as its form is not necessary in the sequel. The soft output of the filter is given by

$$\begin{aligned}\mathbf{z}&=\omega_{\mathrm{mmse}}^H\mathbf{T}\mathbf{y}\\&=\mathbf{A}_1\mathbf{U}_1^H\mathbf{E}_1^{-1}\left[\mathbf{I}\;\middle|\;-\boldsymbol{\Upsilon}_{\mathbf{y}_1\mathbf{d}_1}^H\mathbf{R}_{\mathbf{y}_1}^{-1}\right]\left[\frac{\mathbf{H}_1^H}{\mathbf{B}_1}\right]\mathbf{y}\\&=\mathbf{A}_1\mathbf{U}_1^H\mathbf{E}_1^{-1}\left(\mathbf{d}_1-\omega_1^H\mathbf{y}_1\right)\end{aligned}\quad (17)$$

where

$$\omega_1^{(N-L)\times L}\triangleq\mathbf{R}_{\mathbf{y}_1}^{-1}\boldsymbol{\Upsilon}_{\mathbf{y}_1\mathbf{d}_1}. \quad (18)$$

Now, observe that

$$\begin{aligned}\mathbf{E}_1&=\left(\mathbf{R}_{\mathbf{d}_1}-\boldsymbol{\Upsilon}_{\mathbf{y}_1\mathbf{d}_1}^H\mathbf{R}_{\mathbf{y}_1}^{-1}\boldsymbol{\Upsilon}_{\mathbf{y}_1\mathbf{d}_1}\right)\\&=E\left[\left(\mathbf{d}_1-\omega_1^H\mathbf{y}_1\right)\left(\mathbf{d}_1-\omega_1^H\mathbf{y}_1\right)^H\right].\end{aligned}\quad (19)$$

Therefore, ω_1 is the MMSE FB that minimizes $E\left\|\mathbf{d}_1-\omega_1^H\mathbf{y}_1\right\|^2$, and $\mathbf{E}_1$ is the corresponding error-covariance matrix. Similarly, we can form another unitary matrix $\mathbf{T}_1^{(N-L)\times(N-L)}\triangleq\left[\mathbf{H}_2\,|\,\mathbf{B}_2^H\right]^H$ with $\boldsymbol{\Upsilon}_{\mathbf{y}_1\mathbf{d}_1}=\mathbf{H}_2^{(N-L)\times L}\mathbf{U}_2^{L\times L}$ and $\mathbf{B}_2^{(N-2L)\times(N-L)}\perp\mathbf{H}_2^H$, and still have $E\left\|\mathbf{d}_1-\omega_1^H\mathbf{y}_1\right\|^2=E\left\|\mathbf{d}_1-\omega_1^H\mathbf{T}_1\mathbf{y}_1\right\|^2$. The same procedure from (14)–(17) for calculating ω_{mmse} can also be applied to ω_1, resulting in $\omega_1^H\mathbf{T}_1\mathbf{y}_1=\mathbf{U}_2^H\mathbf{E}_2^{-1}\left(\mathbf{d}_2-\omega_2^H\mathbf{y}_2\right)$, where $\mathbf{d}_2^{L\times 1}=\mathbf{H}_2^H\mathbf{y}_1$, $\mathbf{y}_2^{(N-2L)\times 1}=\mathbf{B}_2\mathbf{y}_1$, $\omega_2^{(N-2L)\times L}=\mathbf{R}_{\mathbf{y}_2}^{-1}\boldsymbol{\Upsilon}_{\mathbf{y}_2\mathbf{d}_2}$, and $\mathbf{E}_2=E\left[\left(\mathbf{d}_2-\omega_2^H\mathbf{y}_2\right)\left(\mathbf{d}_2-\omega_2^H\mathbf{y}_2\right)^H\right]$. Recursively employing the above procedure for $\omega_2^{(N-2L)\times L}$ and the resultant $\omega_3^{(N-3L)\times L}$, $\omega_4^{(N-4L)\times L}$,..., until the dimension N is exhausted, an MS implementation of the MMSE-FB is constructed and shown in Fig. 3. Multiplying the current output of the MS-MMSE-FB with the previous one forms the decision statistic φ in (8). It is noted that the MS-MMSE-FB reduces to the MSWF for the cases of flat-fading channels, in which case, the rank of $\mathbf{H}_1$, L, is equal to one.

B. MS MOE FB

The concept of MS filtering can also be extended to the MOE FB. Recall from (14) that the MSWF differs from the original MMSE by using the transformed received signal $\mathbf{T}\mathbf{y}$, instead of

$\mathbf{y}$, to form the MMSE FB. Motivated by this observation, the MOE criterion in (9) can be reformulated as

$$\omega_{\text{moe}} = \arg\min_{\omega} E\|\omega^H \mathbf{T}\mathbf{y}\|^2 \quad \text{subject to } \omega^H \mathbf{T}\mathbf{S}_{1+}\mathbf{A}_1 = \mathbf{A}_1\mathbf{S}_{1+}^H\mathbf{T}^H\mathbf{T}\mathbf{S}_{1+}\mathbf{A}_1. \quad (20)$$

Let $\mathbf{R}_T = \mathbf{T}\mathbf{R}\mathbf{T}^H$ and $\mathbf{S}_T = \mathbf{T}\mathbf{S}_{1+}$. The optimal FB is given by

$$\omega_{\text{moe}}^{N\times L} = \mathbf{R}_T^{-1}\mathbf{S}_T\left(\mathbf{S}_T^H\mathbf{R}_T^{-1}\mathbf{S}_T\right)^{-1}\mathbf{S}_T^H\mathbf{S}_T\mathbf{A}_1. \quad (21)$$

It is clear that the filter's soft output remains invariant to the unitary transformation $\mathbf{T}$. Using the same transformation matrix $\mathbf{T}$ given by (13) and applying the matrix-inversion lemma to $\mathbf{R}_T^{-1}$, as shown in (16), it is straightforward to show that $\left(\mathbf{S}_T^H\mathbf{R}_T^{-1}\mathbf{S}_T\right)^{-1} = \mathbf{U}_1^{-1}\mathbf{E}_1\mathbf{U}_1^{-H}$. Inserting this result back into (21), and following the same procedure from (16) to (17) for handling the $\mathbf{R}_T^{-1}\mathbf{S}_T$ term, the MOE-FB in (21) can be shown equal to

$$\omega_{\text{moe}}^H = \mathbf{A}_1\mathbf{U}_1^H\left[\mathbf{I} \mid -\boldsymbol{\Upsilon}_{\mathbf{y}_1\mathbf{d}_1}^H\mathbf{R}_{\mathbf{y}_1}^{-1}\right]. \quad (22)$$

The filter's soft output is given by

$$\mathbf{z} = \omega_{\text{moe}}^H\mathbf{T}\mathbf{y} = \mathbf{A}_1\mathbf{U}_1^H\left(\mathbf{d}_1 - \omega_1^H\mathbf{y}_1\right). \quad (23)$$

An important point shown by this formula is that the MS-MMSE-FB in (16) and the MS-MOE-FB in (22) differ only by the matrix $\mathbf{E}_1^{-1}$ in (19), which is a scaling matrix at the filter's output. The MS implementation of the MOE-FB is depicted in Fig. 3.

C. MS Interference Suppressor

Notice from (17) and (23) that ω_1 is a common component filter of both the MS MMSE and MOE implementations. As will be shown later in Section IV, it also plays an important role in the development of the MS-BLUE/ML-FBs. Thus, it is of interest to examine the physical meaning of ω_1. To investigate properties of ω_1, we rewrite the received signal $\mathbf{y}$ as

$$\mathbf{y}(m) = \mathbf{S}_{1+}\mathbf{A}_1\Gamma_1(m)b_1(m) + \mathbf{i}_1(m) \quad (24)$$

where $\mathbf{i}_1^{N\times 1}(m)$ is the interference to the desired user's signal, given by

$$\mathbf{i}_1(m) \triangleq \sum_{k=2}^{K}\sum_{l=1}^{L_k} A_{kl}\gamma_{kl}(m)\mathbf{s}_{kl}^{+}b_k(m-m_{kl}) + \sum_{k=1}^{K}\sum_{l=1}^{L_k} A_{kl}\gamma_{kl}(m)\mathbf{s}_{kl}^{-}b_k(m-m_{kl}-1) + \mathbf{n}(m). \quad (25)$$

The FB ω_1 can be rewritten as $\omega_1 = \mathbf{R}_{\mathbf{y}_1}^{-1}\boldsymbol{\Upsilon}_{\mathbf{y}_1\mathbf{d}_1} = \mathbf{R}_{\mathbf{y}_1}^{-1}E\left(\mathbf{B}_1\mathbf{y}\mathbf{y}^H\mathbf{H}_1\right)$. Since $\mathbf{B}_1\mathbf{y} = \mathbf{B}_1(\mathbf{S}_{1+}\mathbf{A}_1\Gamma_1 b_1 + \mathbf{i}_1) = \mathbf{B}_1\mathbf{i}_1$ and $\mathbf{H}_1^H\mathbf{y} = \mathbf{U}_1\mathbf{A}_1\Gamma_1 b_1 + \mathbf{H}_1^H\mathbf{i}_1$, we can show that

$$E\left(\mathbf{B}_1\mathbf{y}\mathbf{y}^H\mathbf{H}_1\right) = E\left[\left(\mathbf{B}_1\mathbf{i}_1\right)\left(\mathbf{U}_1\mathbf{A}_1\Gamma_1 b_1 + \mathbf{H}_1^H\mathbf{i}_1\right)^H\right] = E\left(\mathbf{B}_1\mathbf{i}_1\mathbf{i}_1^H\mathbf{H}_1\right) \quad (26)$$

using the property that $\mathbf{i}_1$ and b_1 are uncorrelated. Similarly, one can show that $\mathbf{R}_{\mathbf{y}_1} = E\left(\mathbf{B}_1\mathbf{i}_1\mathbf{i}_1^H\mathbf{B}_1^H\right)$, Then, the FB ω_1 is equivalent to the one obtained by the following optimization:

$$\omega_1 = \arg\min_{w} E\left\|\mathbf{H}_1^H\mathbf{i}_1 - \omega^H\mathbf{B}_1\mathbf{i}_1\right\|^2 = \left[E\left(\mathbf{B}_1\mathbf{i}_1\mathbf{i}_1^H\mathbf{B}_1^H\right)\right]^{-1}E\left(\mathbf{B}_1\mathbf{i}_1\mathbf{i}_1^H\mathbf{H}_1\right). \quad (27)$$

Therefore, ω_1 essentially takes the projected interference in the subspace $\mathcal{B}_1$ to suppress the projected interference $\mathbf{H}_1^H\mathbf{i}_1$ in signal subspace $\mathcal{H}_1$, in the sense of the MMSE. In the absence of MAI and intersymbol interference (ISI) such that $\mathbf{i}_1 = \mathbf{n}$, the filter reduces to $\omega_1 = \mathbf{0}$ in (27), due to the fact that $\mathbf{B}_1\mathbf{H}_1 = \mathbf{0}$. There will be no need for the extra stages of the MMSE/MOE FBs other than the first stage, $\mathbf{H}_1$. Thus, $\mathbf{e}_1 \triangleq \left(\mathbf{d}_1 - \omega_1^H\mathbf{y}_1\right)$ functions as an *MS interference suppressor* with the output autocorrelation matrix $\mathbf{E}_1 = E\left(\mathbf{e}_1\mathbf{e}_1^H\right)$. By a similar procedure, the $\mathbf{E}_1$ term in (19) can also be expressed as

$$\mathbf{E}_1 = \left(\mathbf{R}_{\mathbf{d}_1} - \boldsymbol{\Upsilon}_{\mathbf{y}_1\mathbf{d}_1}^H\mathbf{R}_{\mathbf{y}_1}^{-1}\boldsymbol{\Upsilon}_{\mathbf{y}_1\mathbf{d}_1}\right) = \mathbf{U}_1\mathbf{A}_1^2\mathbf{U}_1^H + E\left[\left(\mathbf{H}_1^H\mathbf{i}_1 - \omega_1^H\mathbf{B}_1\mathbf{i}_1\right)\left(\mathbf{H}_1^H\mathbf{i}_1 - \omega_1^H\mathbf{B}_1\mathbf{i}_1\right)^H\right] \quad (28)$$

where $\mathbf{U}_1\mathbf{A}_1^2\mathbf{U}_1^H = \mathbf{H}_1^H\mathbf{S}_{1+}\mathbf{A}_1^2\mathbf{S}_{1+}^H\mathbf{H}_1$ is the autocorrelation matrix of the desired user's signal in signal subspace $\mathcal{H}_1$. So, the matrix $\mathbf{E}_1$ can be interpreted as the desired user's signal covariance matrix, plus the covariance matrix of the residual interference in signal subspace $\mathcal{H}_1$.

IV. MS ML FBs

For coherent detection of BPSK signals where the channel vector Γ_1 is available, the decision statistic is given by $\varphi(m) = \Re\left[\Gamma_1^H(m)\mathbf{z}(m)\right]$ employing MRC. The vector $\mathbf{z}(m)$ is the soft output of the MMSE-based estimator for $b_1\Gamma_1$. In contrast, for noncoherent detection of DBPSK where the channel vector is unknown, the decision statistic is given by $\varphi(m) = \Re[\mathbf{z}^H(m-1)\mathbf{z}(m)]$ employing EGC. In the ideal case, $\mathbf{z}(m) = b_1(m)\Gamma_1(m)$, and thus $\Re[\mathbf{z}^H(m-1)\mathbf{z}(m)] \simeq b_1(m-1)b_1(m)\|\Gamma_1\|^2$. A common interpretation for EGC is that $\mathbf{z}(m-1)$ serves as the channel estimate required by MRC. However, it is noted that conditioned on the channel vector and the data, the MMSE and MOE estimators for $b_1\Gamma_1$ are biased. That is, $E(\mathbf{z}_{\text{mmse}}|\Gamma_1 b_1) = \mathbf{A}_1\mathbf{S}_{1+}^H\mathbf{R}^{-1}\mathbf{S}_{1+}\mathbf{A}_1\Gamma_1 b_1$, and $E(\mathbf{z}_{\text{moe}}|\Gamma_1 b_1) = \mathbf{A}_1\mathbf{S}_{1+}^H\mathbf{S}_{1+}\mathbf{A}_1\Gamma_1 b_1$. We also observe that the bias of the MMSE estimator is a function of system loading through its dependence on $\mathbf{R}$. Furthermore, when MS implementations are employed, the mean values of the MS MMSE/MOE estimator become, respectively

$$E(\mathbf{z}_{\text{mmse}}|\Gamma_1 b_1) = \mathbf{A}_1\mathbf{S}_{1+}^H\mathbf{T}^H \times (\mathbf{T}\mathbf{R}\mathbf{T}^H)^{-1}\mathbf{T}\mathbf{S}_{1+}\mathbf{A}_1\Gamma_1 b_1 \quad (29)$$

$$E(\mathbf{z}_{\text{moe}}|\Gamma_1 b_1) = \mathbf{A}_1\mathbf{S}_{1+}^H\mathbf{T}^H\mathbf{T}\mathbf{S}_{1+}\mathbf{A}_1\Gamma_1 b_1. \quad (30)$$

For full-rank implementations, $\mathbf{T}$ is unitary, i.e., $\mathbf{T}^H\mathbf{T} = \mathbf{I}$, [cf. (13)], the biases are not affected by the transformation. However, as will be shown in Section V, for reduced-rank implementations, $\mathbf{T}$ is replaced by the reduced-rank transformation matrices, e.g., $\mathbf{T}_{LD}$ [cf. (49)], for D-stage implementations,

thus $\mathbf{T}_{LD}^H\mathbf{T}_{LD} \neq \mathbf{I}$. The biases also change with the number of stages of implementations. To eliminate the bias effects, we consider unbiased estimation of $\Gamma_1 b_1$.

A. MS Blue FB

We treat $b_1\Gamma_1$ as a deterministic unknown vector, and aggregate the MAI, ISI, and complex Gaussian noise described in (4), as an interference vector $\mathbf{i}_1$ as given in (24), with covariance matrix $\mathbf{C}_1 = E\left(\mathbf{i}_1\mathbf{i}_1^H\right)$. The BLUE [9] for $b_1\Gamma_1$ can be obtained according to the following criterion:

$$\omega_{\text{blue}}(m) = \arg\min_{\omega} E\left\|\theta_1(m) - \omega_1^H\mathbf{y}(m)\right\|^2 \text{ subject to } E\left(\omega_1^H\mathbf{y}(m)\right) = \theta_1(m) \tag{31}$$

where, to emphasize time dependency and the difference from the MMSE/MOE approaches in which $b_1\Gamma_1$ is a random vector, we define $\theta_1(m) \triangleq b_1(m)\Gamma_1(m)$. The estimate of $\theta_1(m)$ is

$$\begin{aligned}\hat{\theta}_1(m) &= \left(\mathbf{A}_1^H\mathbf{S}_{1+}^H\mathbf{C}_1^{-1}\mathbf{S}_{1+}\mathbf{A}_1\right)^{-1}\mathbf{A}_1^H\mathbf{S}_{1+}^H\mathbf{C}_1^{-1}\mathbf{y}(m)\\ &\triangleq \omega_{\text{blue}}^H\mathbf{y}(m).\end{aligned} \tag{32}$$

Due to the fact that $\mathbf{s}_{kl}^+$ and $\mathbf{s}_{kl}^-$ are deterministic, and Γ_k is a complex Gaussian vector, the interference vector $\mathbf{i}_1(m)$ is a zero-mean, complex-Gaussian distributed vector. Thus, (24) is the Gaussian linear model for $\mathbf{y}$. The ML estimator for $\theta_1(m)$ will attain the Cramer–Rao lower bound (CRLB) [9], and is equivalent to the BLUE estimator given in (32).

We now develop the MS implementation of the BLUE FB. Transforming the received signal $\mathbf{y}(m)$ with the unitary matrix $\mathbf{T}$ given in (13), the resultant signal is of the form

$$\mathbf{T}\mathbf{y} = \mathbf{T}\mathbf{S}_{1+}\mathbf{A}_1\Gamma_1(m)b_1(m) + \mathbf{T}\mathbf{i}_1(m). \tag{33}$$

Let $\mathbf{C}_T \triangleq \mathbf{T}\mathbf{C}_1\mathbf{T}^H$ and $\mathbf{S}_T \triangleq \mathbf{T}\mathbf{S}_{1+}$. The BLUE/ML estimator for $\theta_1(m)$ is given by

$$\begin{aligned}\hat{\theta}_1(m) &= \left(\mathbf{A}_1\mathbf{S}_T^H\mathbf{C}_T^{-1}\mathbf{S}_T\mathbf{A}_1\right)^{-1}\mathbf{A}_1\mathbf{S}_T^H\mathbf{C}_T^{-1}\mathbf{T}\mathbf{y}(m)\\ &= \left(\mathbf{A}_1\mathbf{S}_{1+}^H\mathbf{C}_1^{-1}\mathbf{S}_{1+}\mathbf{A}_1\right)^{-1}\mathbf{A}_1\mathbf{S}_{1+}^H\mathbf{C}_1^{-1}\mathbf{y}(m).\end{aligned} \tag{34}$$

The equality can be easily verified, since $\mathbf{T}^H = \mathbf{T}^{-1}$. Like the MS MMSE/MOE-FBs, a unitary transformation does not change the estimation result. Now, we apply the matrix-inversion lemma [9] to $\left(\mathbf{T}\mathbf{C}_1\mathbf{T}^H\right)^{-1}$, such that

$$\begin{aligned}&(\mathbf{T}\mathbf{C}_1\mathbf{T}^H)^{-1}\\ &\quad= \left(\begin{bmatrix}\mathbf{H}_1^H\\ \hline \mathbf{B}_1\end{bmatrix}\mathbf{C}_1\begin{bmatrix}\mathbf{H}_1 & \vert & \mathbf{B}_1^H\end{bmatrix}\right)^{-1}\\ &\quad= \left[\begin{array}{c|c}\mathbf{K}_{\mathbf{i}_{H_1}} & \boldsymbol{\Upsilon}_{\mathbf{i}_{B_1}\mathbf{i}_{H_1}}^H\\ \hline \boldsymbol{\Upsilon}_{\mathbf{i}_{B_1}\mathbf{i}_{H_1}} & \mathbf{K}_{\mathbf{i}_{B_1}}\end{array}\right]^{-1}\\ &\quad= \left[\begin{array}{c|c}\mathbf{F}_1^{-1} & -\mathbf{F}_1^{-1}\boldsymbol{\Upsilon}_{\mathbf{i}_{B_1}\mathbf{i}_{H_1}}^H\mathbf{K}_{\mathbf{i}_{B_1}}^{-1}\\ \hline -\mathbf{K}_{\mathbf{i}_{B_1}}^{-1}\boldsymbol{\Upsilon}_{\mathbf{i}_{B_1}\mathbf{i}_{H_1}}\mathbf{F}_1^{-1} & \Delta\end{array}\right]\end{aligned} \tag{35}$$

where $\mathbf{i}_{H_1} \triangleq \mathbf{H}_1^H\mathbf{i}_1$, $\mathbf{i}_{B_1} \triangleq \mathbf{B}_1\mathbf{i}_1$; $\mathbf{K}_{\mathbf{i}_{H_1}}$ and $\mathbf{K}_{\mathbf{i}_{B_1}}$ are the autocovariance matrices of $\mathbf{i}_{H_1}$ and $\mathbf{i}_{B_1}$, respectively, $\boldsymbol{\Upsilon}_{\mathbf{i}_{B_1}\mathbf{i}_{H_1}} \triangleq E\left(\mathbf{i}_{B_1}\mathbf{i}_{H_1}^H\right)$ is the cross-covariance matrix of $\mathbf{i}_{B_1}$ and $\mathbf{i}_{H_1}$, and

$$\mathbf{F}_1 \triangleq \mathbf{K}_{\mathbf{i}_{H_1}} - \boldsymbol{\Upsilon}_{\mathbf{i}_{B_1}\mathbf{i}_{H_1}}^H\mathbf{K}_{\mathbf{i}_{B_1}}^{-1}\boldsymbol{\Upsilon}_{\mathbf{i}_{B_1}\mathbf{i}_{H_1}}. \tag{36}$$

Inserting (35) back into (34), the BLUE estimator can be simplified to

$$\begin{aligned}\hat{\theta}_1(m) &= \left(\mathbf{A}_1\mathbf{U}_1^H\mathbf{F}_1^{-1}\mathbf{U}_1\mathbf{A}_1\right)^{-1}\mathbf{A}_1\mathbf{U}_1^H\mathbf{F}_1^{-1}\\ &\quad\times\left(\mathbf{H}_1^H - \boldsymbol{\Upsilon}_{\mathbf{i}_{B_1}\mathbf{i}_{H_1}}^H\mathbf{K}_{\mathbf{i}_{B_1}}^{-1}\mathbf{B}_1\right)\mathbf{y}(m)\\ &= \mathbf{A}_1^{-1}\mathbf{U}_1^{-1}\left(\mathbf{H}_1^H - \boldsymbol{\Upsilon}_{\mathbf{i}_{B_1}\mathbf{i}_{H_1}}^H\mathbf{K}_{\mathbf{i}_{B_1}}^{-1}\mathbf{B}_1\right)\mathbf{y}(m)\\ &= \mathbf{A}_1^{-1}\mathbf{U}_1^{-1}\left(\mathbf{d}_1 - \boldsymbol{\Upsilon}_{\mathbf{i}_{B_1}\mathbf{i}_{H_1}}^H\mathbf{K}_{\mathbf{i}_{B_1}}^{-1}\mathbf{y}_1\right)\end{aligned} \tag{37}$$

where $\mathbf{d}_1 \triangleq \mathbf{H}_1^H\mathbf{y}$ and $\mathbf{y}_1 \triangleq \mathbf{B}_1\mathbf{y}$. As has been shown in (26), $\boldsymbol{\Upsilon}_{\mathbf{i}_{B_1}\mathbf{i}_{H_1}} \triangleq E\left(\mathbf{B}_1\mathbf{i}_1\mathbf{i}_1^H\mathbf{H}_1\right) = \boldsymbol{\Upsilon}_{\mathbf{y}_1\mathbf{d}_1}$ and $\mathbf{K}_{\mathbf{i}_{B_1}} \triangleq E\left(\mathbf{B}_1\mathbf{y}\mathbf{y}^H\mathbf{B}_1^H\right) = \mathbf{R}_{\mathbf{y}_1}$, the BLUE estimator is equal to

$$\begin{aligned}\hat{\theta}_1(m) &= \mathbf{A}_1^{-1}\mathbf{U}_1^{-1}\left(\mathbf{d}_1 - \boldsymbol{\Upsilon}_{\mathbf{y}_1\mathbf{d}_1}^H\mathbf{R}_{\mathbf{y}_1}^{-1}\mathbf{y}_1\right)\\ &= \mathbf{A}_1^{-1}\mathbf{U}_1^{-1}\left(\mathbf{d}_1 - \omega_1^H\mathbf{y}_1\right).\end{aligned} \tag{38}$$

Furthermore, $\mathbf{R}_{\mathbf{d}_1} = \mathbf{U}_1\mathbf{A}_1^2\mathbf{U}_1^H + \mathbf{K}_{\mathbf{i}_{H_1}}$. By (28) and (36), we have

$$\begin{aligned}\mathbf{F}_1 &= \mathbf{K}_{\mathbf{i}_{H_1}} - \boldsymbol{\Upsilon}_{\mathbf{y}_1\mathbf{d}_1}^H\mathbf{R}_{\mathbf{y}_1}^{-1}\boldsymbol{\Upsilon}_{\mathbf{y}_1\mathbf{d}_1}\\ &= E\left[\left(\mathbf{H}_1^H\mathbf{i}_1 - \omega_1^H\mathbf{B}_1\mathbf{i}_1\right)\left(\mathbf{H}_1^H\mathbf{i}_1 - \omega_1^H\mathbf{B}_1\mathbf{i}_1\right)^H\right]\\ &= \mathbf{E}_1 - \mathbf{U}_1\mathbf{A}_1^2\mathbf{U}_1^H.\end{aligned} \tag{39}$$

Again, $\omega_1 \triangleq \mathbf{R}_{\mathbf{y}_1}^{-1}\boldsymbol{\Upsilon}_{\mathbf{y}_1\mathbf{d}_1}$ plays a crucial role for the MS BLUE. The BLUE-FB shares the same MS interference suppressor, $\left[\mathbf{d}_1 - \omega_1^H\mathbf{y}_1\right]$, with the MMSE/MOE-FBs, with a distinctive scaling matrix $\mathbf{A}_1^{-1}\mathbf{U}_1^{-1}$. Thus, the implementation is straightforward, as shown in Fig. 3.

Now, we have the MS BLUE-FB as an unbiased "channel" estimator of $\Gamma_1 b_1$. It is not difficult to show that the covariance matrices for the MS MMSE/BLUE-FBs conditioned on $\Gamma_1 b_1$ are given by

$$\begin{aligned}\text{Cov}(\mathbf{z}_{\text{mmse}}|\Gamma_1 b_1) &= \mathbf{A}_1\mathbf{U}_1^H\mathbf{E}_1^{-1}\mathbf{U}_1\mathbf{A}_1\\ &\quad - \left(\mathbf{A}_1\mathbf{U}_1^H\mathbf{E}_1^{-1}\mathbf{U}_1\mathbf{A}_1\right)^2\end{aligned} \tag{40}$$

$$\text{Cov}(\mathbf{z}_{\text{blue}}|\Gamma_1 b_1) = \mathbf{A}_1^{-1}\mathbf{U}_1^{-H}\mathbf{E}_1\mathbf{U}_1^{-H}\mathbf{A}_1^{-1} - \mathbf{I}. \tag{41}$$

Let $\mathbf{A}_1\mathbf{U}_1^H\mathbf{E}_1^{-1}\mathbf{U}_1\mathbf{A}_1 = \mathbf{Q}\Lambda\mathbf{Q}^H$. By (40) and the positive definiteness of a covariance matrix, it is straightforward to show that $\mathbf{0} \leq \Lambda \leq \mathbf{I}$. Thus, we have

$$\begin{aligned}&\text{Cov}(\mathbf{z}_{\text{blue}}|\Gamma_1 b_1) - \text{Cov}(\mathbf{z}_{\text{mmse}}|\Gamma_1 b_1)\\ &\quad= \mathbf{Q}[\Lambda^{-1}(\Lambda + \mathbf{I})(\Lambda - \mathbf{I})^2]\mathbf{Q}^H \geq \mathbf{0}.\end{aligned} \tag{42}$$

So the BLUE-FB, while unbiased, exhibits a larger estimation variance than that of the MMSE-FB. However, for the roles of the channel estimator and the data detector in MRC/EGC methods, there are different sensitivities to the bias and the variance. Both of these effects will be studied via simulation, in the context of adaptive coherent detection for BPSK and noncoherent detection for DBPSK.

B. MS ML FB

So far, we have the MS BLUE-FB as an implicit ML channel estimator for EGC. What is missing is a MS FB for ML symbol detection, although the BLUE-FB can serve as a detector, as can

the MS MMSE/MOE-FBs. Given that the ML detector maximizes the SINR conditioned on $\Gamma_1 b_1$ [10], it should provide better performance.

We consider the blind ML MUD. Given that $\mathbf{i}_1$ in (24) is Gaussian distributed, the probability density function (pdf) of $\mathbf{y}$ conditioned on $\Gamma_1 b_1$ is of the form

$$\mathcal{P}(\mathbf{y}|\Gamma_1 b_1) = \frac{1}{\pi^N \det(\mathbf{C}_1)} \exp\Big\{-(\mathbf{y} - \mathbf{S}_{1+}\mathbf{A}_1\Gamma_1 b_1)^H \mathbf{C}_1^{-1} \times (\mathbf{y} - \mathbf{S}_{1+}\mathbf{A}_1\Gamma_1 b_1)\Big\}. \quad (43)$$

The ML symbol detector is given by

$$\begin{aligned}\hat{b}_1(m) &= \operatorname{sgn}\left\{\Re\left[\Gamma_1^H(m)\mathbf{A}_1\mathbf{S}_{1+}^H\mathbf{C}_1^{-1}\mathbf{y}(m)\right]\right\} \\ &\triangleq \operatorname{sgn}\left\{\Re\left[\Gamma_1^H(m)\omega_{ml}^H(m)\mathbf{y}(m)\right]\right\}. \end{aligned} \quad (44)$$

Similarly, for the transformed signal $\mathbf{Ty}$, the soft output of the ML-FB is given by

$$\begin{aligned}\mathbf{z}_{\rm ml} &= \mathbf{A}_1\mathbf{S}_{1+}^H\mathbf{T}^H\left(\mathbf{T}\mathbf{C}_1\mathbf{T}^H\right)^{-1}\mathbf{T}\mathbf{y} \\ &= \mathbf{A}_1\mathbf{U}_1^H\mathbf{F}_1^{-1}\left(\mathbf{d}_1 - \boldsymbol{\Upsilon}_{\mathbf{y}_1\mathbf{d}_1}^H\mathbf{R}_{\mathbf{y}_1}^{-1}\mathbf{y}_1\right) \end{aligned} \quad (45)$$

where the results from (35)–(39) have been used for the above simplifications, and $\mathbf{F}_1 = \mathbf{E}_1 - \mathbf{U}_1\mathbf{A}_1^2\mathbf{U}_1^H$, [cf. (39)]. The same MS structure for the MMSE-FB also applies to the blind ML detector by replacing the output scaling matrix $\mathbf{E}_1$ with $\mathbf{F}_1$.

V. Reduced-Rank MS Multiuser Receivers

A. Common Structure for MRC/EGC MUD

It is clear now that the MS MMSE/MOE/BLUE/ML FBs all share a common MS interference suppressor, $\left(\mathbf{d}_1 - \omega_1^H\mathbf{y}_1\right)$, with distinctive scaling matrices. The filters' soft outputs can be represented with a common form

$$\begin{aligned}\mathbf{z}_i &\triangleq \omega_i^H\mathbf{T}\mathbf{y} \\ &= \mathbf{C}_i\left(\mathbf{d}_1 - \boldsymbol{\Upsilon}_{\mathbf{y}_1\mathbf{d}_1}^H\mathbf{R}_{\mathbf{y}_1}^{-1}\mathbf{y}_1\right), \quad i \in \{\text{mmse, moe, blue, ml}\} \end{aligned} \quad (46)$$

with $\mathbf{C}_{\rm mmse} \triangleq \mathbf{A}_1\mathbf{U}_1^H\mathbf{E}_1^{-1}$, $\mathbf{C}_{\rm moe} \triangleq \mathbf{A}_1\mathbf{U}_1^H$, $\mathbf{C}_{\rm blue} \triangleq \mathbf{A}_1^{-1}\mathbf{U}_1^{-1}$, and $\mathbf{C}_{\rm ml} \triangleq \mathbf{A}_1\mathbf{U}_1^H\mathbf{F}_1^{-1}$. Different filters scale the output of the MS interference suppressor with different matrices to achieve their specific optimization criteria, e.g., MOE is equivalent to minimizing $\omega^H E\left(\mathbf{i}_1\mathbf{i}_1^H\right)\omega$.

The computational complexity for the common MS interference suppressor of D stages is $D[O(L^2) + O(LN)]$, $DL \leq N$, as opposed to the complexity of $O(N^2) + O(LN)$ for the traditional implementation of the MMSE-FB. As is usually the case for DS-CDMA channels, N is much greater than L, and a significant amount of implementation cost can be saved for the proposed reduced-rank MS implementation without sacrificing output performance. Moreover, with this common structure, one can easily build different filters for specific applications without employing redundant implementation logics for each filter. With the aid of this specific characteristic, we have a common framework for the implementation of coherent MRC and noncoherent EGC detection of DS-CDMA systems, as shown in Fig. 1. For MRC schemes, the block of estimation scaling is removed and replaced by the known channel vector Γ_1.

Despite the fact that a number of detection schemes can be implemented and evaluated using the same common framework with different matrices for $\mathbf{C}_{\rm Est}$ and $\mathbf{C}_{\rm Det}$, as shown in Fig. 1, we highlight a specific noncoherent EGC receiver with the decision statistic given by

$$\varphi(m) = \Re\left[\mathbf{z}_{\rm blue}^H(m-1)\mathbf{z}_{\rm ml}(m)\right]. \quad (47)$$

Recall that the BLUE-FB acts as an implicit ML channel estimator for EGC, and the ML-FB is a ML symbol detector. Therefore, this receiver scheme is referred to as EGC of the ML FBs (EGC-ML-FB).

It appears that bias in the channel estimate can have a deleterious effect on overall performance, and thus, the BLUE channel estimator offers superior performance; similarly, the ML detection strategy most directly optimizes the detection error. Thus, employing the best channel-estimation method with the best detection method offers the best combined performance. This is confirmed via simulation in Fig. 11. The implementation of the EGC-ML-FB can be achieved by having $\mathbf{C}_{\rm Est} = \mathbf{C}_{\rm blue}$ and $\mathbf{C}_{\rm Det} = \mathbf{C}_{\rm ml}$ in Fig. 1. Different from the EGC MMSE/MOE/BLUE FBs, where outputs of the same FB are combined with equal gain, the EGC-ML-FB is a *heterogeneous* combining of two different types of FBs' outputs.

B. Reduced-Rank MS Interference Suppressor

To improve the tracking performance and reduce the variance of the estimation error in dynamic channel environments, reduced-rank implementations are often considered for MMSE estimation. For MSWF, a transformation matrix for its reduced-rank implementation was given in [3]. The performance of MSWF was later shown in [11] to be independent of the choice of the blocking matrix $\mathbf{B}_1$ embedded in the transformation matrix. For the MS FBs introduced in this paper, reduced-rank implementations also follow the same rule for the MSWF by keeping the first D stages of the MS FBs. The basis vectors for the reduced-rank MS FBs are the same, because the common MS interference suppressor for these FBs is constructed with the same set of basis vectors. Let $\mathcal{T}_{LD}$ denote the subspace spanned by the basis vectors for the D-stage MS interference suppressor. The matrix $\mathbf{T}_{LD}$ of the basis vectors is given by *Proposition 1*, and the proof is provided in the Appendix. The subspace $\mathcal{T}_{LD}$ is a generalization of the subspace associated with the MSWF given in [3].

Proposition 1: The basis vectors for the MS MMSE/MOE/BLUE/ML FBs.

1) Let the blocking matrix $\mathbf{B}_i$ at each stage i in Fig. 3 be constructed by $\mathbf{B}_i^{N\times N} \triangleq \mathbf{I} - \mathbf{H}_i\mathbf{H}_i^H$. A recursive procedure for generating the matched FBs $\mathbf{H}_i^{N\times L}$ at each stage i is given as follows, with the matched filter of the first stage, $\mathbf{H}_1 = \mathbf{S}_{1+}\mathbf{A}_1\mathbf{U}_1^{-1}$:

$$\begin{aligned}\mathbf{H}_i^{N\times L}\mathbf{U}_i^{L\times L} &= E\left(\mathbf{y}_{i-1}\mathbf{d}_{i-1}^H\right) \\ &= \mathbf{B}_{i-1}E\left(\mathbf{y}_{i-2}\mathbf{y}_{i-2}^H\right)\mathbf{H}_{i-1} \\ &= \prod_{j=(i-1)}^{1}\left(\mathbf{I} - \mathbf{H}_j\mathbf{H}_j^H\right)\mathbf{R}\mathbf{H}_{i-1}, \quad i = 2\ldots D \end{aligned} \quad (48)$$

where $\mathbf{y}_i = \mathbf{B}_i\mathbf{y}_{i-1}$, $\mathbf{d}_i = \mathbf{H}_i^H\mathbf{y}_{i-1}$, and $\mathbf{y}_0 \triangleq \mathbf{y}$. $\mathbf{H}_i^H\mathbf{H}_i = \mathbf{I}$ and $\mathbf{H}_i \perp \mathbf{H}_j$, $i \neq j$, $i = 1\ldots D$.

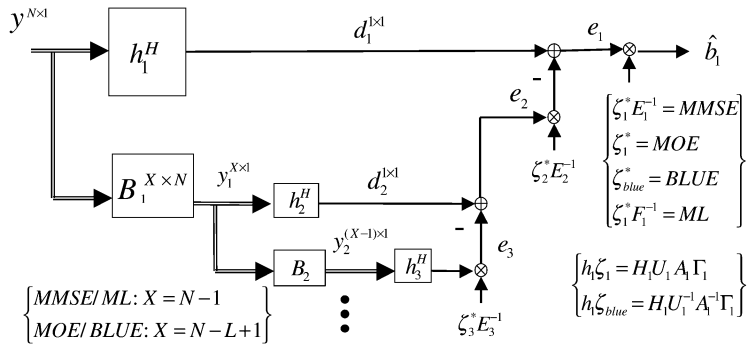

Fig. 4. Structure of the PC MMSE/MOE/ML/BLUE filters, where $\mathbf{h}_1\zeta_1 = \mathbf{S}_{1+}\mathbf{A}_1\Gamma_1$ for the PC MMSE/MOE/ML filters, and $\mathbf{h}_1\zeta_{\text{blue}} = \mathbf{H}_1\mathbf{U}_1^{-1}\mathbf{A}_1^{-1}\Gamma_1$ for the PC-BLUE filter. Dimension of the blocking matrix $\mathbf{B}_1$ is $(N-1)\times N$ for the PC MMSE/ML filters, and $(N-L+1)\times N$ for the PC MOE/BLUE filters. Output scaling value is $\zeta_1^*\mathbf{E}_1^{-1}$ for the PC-MMSE filter, ζ_1^* for the PC-MOE, ζ_{blue}^* for the PC-BLUE, and $\zeta_1^*\mathbf{F}_1^{-1}$ for the PC-ML filter. The objective of estimation is b_1.

2) The basis vectors which span the subspace, $\mathcal{T}_{LD}$, for the reduced-rank FBs of D stages are given by the row vectors of the transformation matrix $\mathbf{T}_{LD}^{LD\times N}$ of the form

$$\begin{aligned}\mathbf{T}_{LD}^H &= \left[\mathbf{H}_1 \mid \mathbf{B}_1\mathbf{H}_2 \mid \cdots \mid \prod_{i=1}^{D-1}\mathbf{B}_i\mathbf{H}_D\right] \\ &= [\mathbf{H}_1 \mid \mathbf{H}_2 \mid \cdots \mid \mathbf{H}_D]. \end{aligned} \tag{49}$$

The reduced-rank implementation of the MS MMSE/MOE/BLUE/ML FBs is equivalent to replacing the transformation matrix $\mathbf{T}$ in (15), (21), (34), and (45) by $\mathbf{T}_{LD}$.

VI. MS Precombining Filters for Coherent Detection

It is clear from *Proposition 1* that the entire implementation structure for the MS receivers proposed herein depends on the steering matrix $\mathbf{H}_1$ and the autocorrelation matrix $\mathbf{R}$, which are relatively stationary, compared with the channel coefficient vector Γ_1. Once the matrices $\mathbf{H}_1$ and $\mathbf{R}$ are available, MUD can be realized without the knowledge of explicit CSI, using EGC in conjunction with differential encoding/decoding. If the CSI is somehow available in real time using training symbols or a pilot channel, then MRC FBs can serve the task of MUD. It is noted that the MS structure for interference suppression does not change before the next updates for matrices $\mathbf{H}_1$ and $\mathbf{R}$, even if the channel coefficients may change every symbol time. The reason is that MAI and ISI are mitigated before the multipath combining using EGC or MRC. The interference residing in each basis vector of the signal subspace $\mathcal{H}_1$ is jointly suppressed with the MS interference suppressor. However, as opposed to this postcombining approach that underlies the EGC/MRC receivers, multipath combining could also be done before interference suppression if CSI is available. This precombining (PC) strategy leads to a set of MS PC filters for coherent detection as well, at a higher cost for MS implementations in time-varying multipath channels. Before we compare and contrast MRC and PC approaches, we shall first introduce the MS PC MMSE, MOE, BLUE, and ML filters, as well as their reduced-rank implementations. We start with the PC MOE and BLUE filters, because these two filters can be directly derived from their MRC counterparts.

A. MS PC MOE/BLUE Filters

Given the desired user's channel parameter Γ_1, (23) and (38) for the MS MOE and BLUE FBs, respectively, can be further simplified by merging the channel parameter Γ_1 with the output scaling matrix as shown below, since $\mathbf{A}_1$ and $\mathbf{U}_1$ are constant matrices

$$\begin{aligned} z_{\text{moe}} &= \Gamma_1^H\mathbf{A}_1\mathbf{U}_1^H\left(\mathbf{d}_1 - \boldsymbol{\Upsilon}_{\mathbf{y}_1\mathbf{d}_1}^H\mathbf{R}_{\mathbf{y}_1}^{-1}\mathbf{y}_1\right) \\ &= \left(d_{11} - \underline{\omega}_{11}^H\mathbf{y}_1\right) \end{aligned} \tag{50}$$

$$\begin{aligned} z_{\text{blue}} &= \Gamma_1^H\mathbf{A}_1^{-1}\mathbf{U}_1^{-H}\left(\mathbf{d}_1 - \boldsymbol{\Upsilon}_{\mathbf{y}_1\mathbf{d}_1}^H\mathbf{R}_{\mathbf{y}_1}^{-1}\mathbf{y}_1\right) \\ &= \left(d_{12} - \underline{\omega}_{12}^H\mathbf{y}_1\right). \end{aligned} \tag{51}$$

The corresponding variables are defined as $d_{11} \triangleq \Gamma_1^H\mathbf{A}_1\mathbf{U}_1^H\mathbf{H}_1^H\mathbf{y}$, $d_{12} \triangleq \Gamma_1^H\mathbf{A}_1^{-1}\mathbf{U}_1^{-H}\mathbf{H}_1^H\mathbf{y}$, $\underline{\omega}_{11} \triangleq \mathbf{R}_{\mathbf{y}_1}^{-1}E(\mathbf{y}_1 d_{11}^*)$, and $\underline{\omega}_{12} \triangleq \mathbf{R}_{\mathbf{y}_1}^{-1}E(\mathbf{y}_1 d_{12}^*)$. The MRC MOE/BLUE FBs with the steering matrix $\mathbf{H}_1$ are equivalent to the filters obtained by using the PC steering vectors $\Gamma_1^H\mathbf{A}_1\mathbf{U}_1^H\mathbf{H}_1^H$ and $\Gamma_1^H\mathbf{A}_1^{-1}\mathbf{U}_1^{-H}\mathbf{H}_1^H$ of dimension $N\times 1$, respectively. They are referred to as the PC MOE/BLUE filters. Their MS implementations are shown in Fig. 4. With a similar procedure for proving *Proposition 1*, it is straightforward to show that the subspace, denoted by $\mathcal{T}_{L+D-1}$, spanned by the basis vectors for the D-stage PC MOE/BLUE filters, is equal to the row space of the matrix $\mathbf{T}_{L+D-1}^{(L+D-1)\times N}$ given by

$$\begin{aligned} \mathbf{T}_{L+D-1}^H &= [\mathbf{H}_1 \mid \mathbf{h}_2 \mid \cdots \mid \mathbf{h}_D] \\ \mathbf{h}_i^{N\times 1}\zeta_i &= E(\mathbf{y}_{i-1}d_{i-1}^*) \\ &= \mathbf{B}_{i-1}E\left(\mathbf{y}_{i-2}\mathbf{y}_{i-2}^H\right)\mathbf{h}_{i-1} \\ &= \prod_{j=(i-1)}^{2}\left(\mathbf{I} - \mathbf{h}_j\mathbf{h}_j^H\right) \\ &\quad \times \left(\mathbf{I} - \mathbf{H}_1\mathbf{H}_1^H\right)\mathbf{R}\mathbf{h}_{i-1}, \quad i = 2\ldots D \\ \text{and } \mathbf{h}_i^H\mathbf{h}_i = 1, &\quad \mathbf{h}_i \perp \mathbf{H}_1 \quad \forall\, i, \quad \mathbf{h}_i \perp \mathbf{h}_j, \quad i \neq j \end{aligned} \tag{52}$$

where $\mathbf{B}_1 = \left(\mathbf{I} - \mathbf{H}_1\mathbf{H}_1^H\right)$ and $\mathbf{B}_i = \left(\mathbf{I} - \mathbf{h}_i\mathbf{h}_i^H\right)$, $i = 2,\ldots D$. We emphasize that the subspaces for the PC-MOE and the PC-BLUE filters are, in essence, different due to the structural differences after the second stage of these two filters. The reason is that their steering vectors are not

the same: $\mathbf{h}_1\zeta_1 = \mathbf{H}_1\mathbf{U}_1\mathbf{A}_1\Gamma_1$ for the PC-MOE filter, and $\mathbf{h}_1\zeta_{\text{blue}} = \mathbf{H}_1\mathbf{U}_1^{-1}\mathbf{A}_1^{-1}\Gamma_1$ for the PC-BLUE filter. The rank for each vector $\mathbf{h}_i$, $i = 2 \ldots D$, is one. The total rank for the D-stage implementations of the PC MOE/BLUE filters is $L + D - 1$, instead of LD as for the MRC MOE/BLUE FBs.

B. MS PC MMSE/ML Filters

For the cases of the MMSE/ML FBs, the output scaling matrices $\mathbf{E}_1$ in (19) for the MMSE-FB, and $\mathbf{F}_1$ in (39) for the ML-FB, are functions of $\mathbf{R}$ and the number of stages that is also revealed in the rank of $\mathbf{T}_{LD}$. Therefore, the PC MMSE/ML filters are, in essence, different from the MRC MMSE/ML FBs. The PC-MMSE filter is exactly the MSWF proposed in [1], with the steering vector equal to $\mathbf{h}_1\zeta_1 = \mathbf{S}_{1+}A_1\Gamma_1$. The PC-ML filter is equal to the MSWF by replacing the output scaling $\mathbf{F}_1$ with $\mathbf{E}_1$.[1] Their MS implementations are also shown in Fig. 4. The subspace $\mathcal{T}_D$ associated with the D-stage implementations of these two filters is equal to the row space of $\mathbf{T}_D^{D\times N}$ of the form [3]

$$\mathbf{T}_D^H = [\mathbf{h}_1 \mid \mathbf{h}_2 | \cdots | \mathbf{h}_D], \quad \mathbf{h}_1\zeta_1 = \mathbf{S}_{1+}A_1\Gamma_1. \tag{53}$$

The total rank of the D-stage PC MMSE/ML filters is D. The extra dimensions for the reduced-rank PC MOE/BLUE filters are used to satisfy the constraints for optimization.

C. MRC Versus PC

Comparing the MRC FBs and PC filters, it is clear that the underlying subspaces defined by these two approaches have distinctly different dimensions, given the same number of stages. As has been shown at the beginning of Section VI, the dimensional difference is due to the fact that PC coherently combines with the channel coefficients prior to interference suppression, while MRC does so after interference suppression. By exploiting the structural invariance of the MS interference suppressor, a common framework is developed in Section V-A for coherent MRC or noncoherent EGC MUD. While, for PC filters, the steering vectors are functions of the channel coefficients, as well. As the process of constructing the filters continues down the MS hierarchy, as shown in (52) and (53), the channel coefficients will be involved in every stage of the filters. Due to this difference, the PC-based interference suppressors change with the channel coefficients, while the MRC-based schemes do not. The MS interference suppressor of a PC filter has to be reconstructed whenever the channel coefficients get updated. Moreover, due to the differences in forming the steering vectors, as shown in (50) and (51), there does not exist a unified framework for the interference suppression of PC filters.

Another advantage for MRC is its flexibility for performance analysis. By decoupling the channel coefficients from the MS structure for interference suppression, we are able to define the signal subspace $\mathcal{H}_1$, and its orthogonal complement subspace $\mathcal{B}_1$ associated with the MRC FBs, separately from the realizations of channel coefficients. By evaluating the channel variation and the capability for interference suppression, as revealed in the recursive structure of the receiver, separately, we can proceed with the performance analysis for coherent MRC or noncoherent EGC MS receivers in multipath Rayleigh fading channels more easily. The analytical results for the output SINRs and bit-error rates (BERs) are presented in [12]. Hence, the common structure presented in Fig. 1 is an efficient framework for both practical implementation and performance analysis.

On the other hand, for PC filters, the channel coefficients are encapsulated in every stage of the filters, making performance analysis extremely complicated for fading channels. The advantage of PC is more pronounced if the channel coefficients are time invariant or more stationary. This is not simply because of the practical consideration. With the assumption of stationary channel coefficients, the subspace spanned by the steering vector of a PC filter has a concrete geometric meaning. Otherwise, it is ambiguous to define a subspace that is spanned by a steering vector with mean zero, due to the zero-mean channel coefficients involved in the vector.

Nevertheless, PC is still useful in certain scenarios. As has been shown in Section III-C, the MS interference suppressor takes the projected interference onto the subspace $\mathcal{B}_1$ to suppress the interference in the signal subspace $\mathcal{H}_1$. If the channel coefficients are not given *a priori*, then interference in each vector subspace of $\mathcal{H}_1$ needs to be suppressed before EGC or MRC. However, for PC filtering, an interference suppressor only needs to mitigate the interference along the composite signal subspace, given the channel vector Γ_1. As a result, the ranks of the MRC MMSE/ML filters and the MRC MOE/BLUE filters can be drastically reduced from LD to D and $L + D - 1$, respectively. With this dimensional reduction, the output SINRs of the PC filters will converge faster than those of the MRC FBs, as will be shown in simulation results. This will enhance the receivers' adaptive performance for nonstationary system loadings, where the received signal's autocorrelation matrix $\mathbf{R}$ changes with time.

VII. Simulation Results

Simulations have been conducted to study the performance of the MS MRC MMSE/MOE/BLUE/ML FBs for coherent detection of BPSK-modulated DS-CDMA systems, and the performance of the MS EGC MMSE/MOE/BLUE/ML FBs for noncoherent detection of DBPSK-modulated systems. A short-code DS-CDMA system with spreading gains $N = 31$ or $N = 64$ is considered. The signature sequences are either randomly generated for investigating the average output SINRs, or randomly chosen from a set of Gold codes, to demonstrate the BER performance. The simulation channel for each user is a three-path (i.e., $L = 3$) Rayleigh fading channel with the normalized Doppler shift $f_dT_s = 5 \times 10^{-3}$. The path delay τ_{kl} for each user is randomly generated with uniform distribution over $[0, 2T_s)$ subject to the constraint that the delay spread satisfies: $|\max_l\{\tau_{kl}\} - \min_l\{\tau_{kl}\}| < \tau_{\max}$, where $\tau_{\max} \leq T_s$ is defined as the maximum allowable delay spread for all users, and serves as an experimental parameter for investigating detectors' performance. The sensitivities of the output SINRs to different amounts of maximum delay spreads $\tau_{\max}$ are investigated via simulations, and presented in the following results. There are 10 users in the system, and all are assumed to have the

[1]Matrices $\mathbf{E}_1$ and $\mathbf{F}_1$ are scalar in this case, since the rank of the steering vector $\mathbf{S}_{1+}A_1\Gamma_1$ is one.

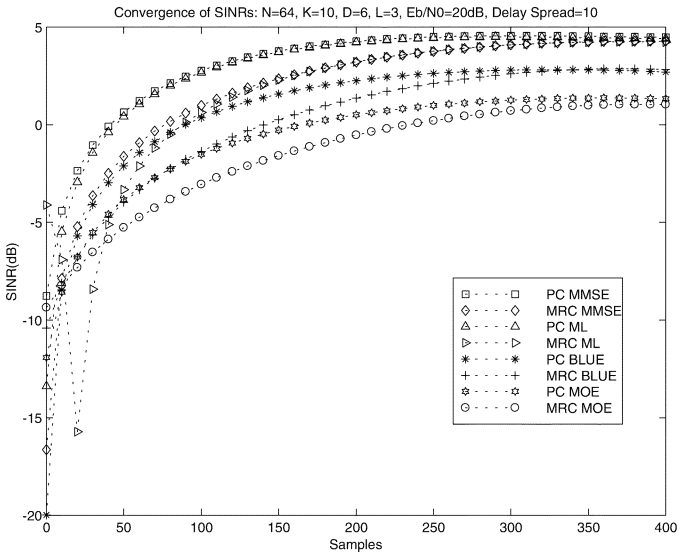

Fig. 5. Convergence characteristics of the output SINRs of the adaptive reduced-rank MRC versus PC MMSE/MOE/BLUE/ML filters for BPSK-modulated signal over a Rayleigh fading channel, with $L = 3$ and the normalized Doppler shift $f_dT_s = 5 \times 10^{-3}$. Maximum allowable delay spread $\tau_{\max} = 10$ chips for all users, and $K = 10$. Number of stages is $D = 6$ for all reduced-rank filters.

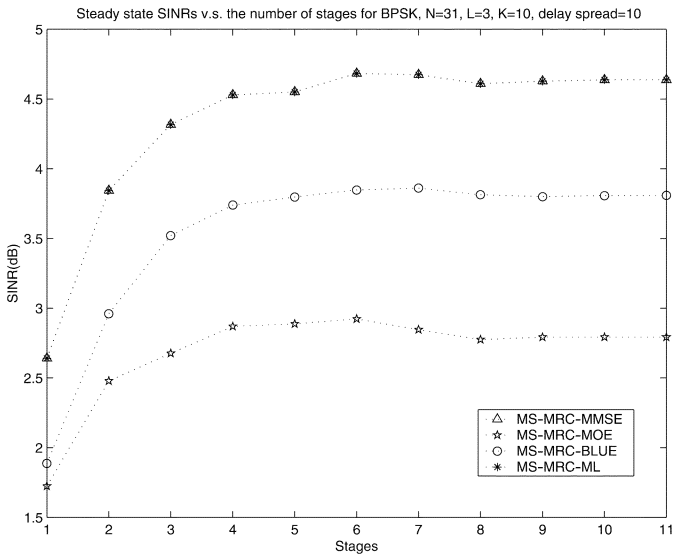

Fig. 6. Steady-state output SINRs of the adaptive reduced-rank MRC MMSE/MOE/BLUE/ML FBs versus the number of stages for BPSK-modulated signals over a Rayleigh fading channel, with the number of paths $L = 3$, and the normalized Doppler shift $f_dT_s = 5 \times 10^{-3}$. Stage 11 in the plot corresponds to the full-rank $(N = 31)$ SINRs. Maximum allowable delay spread $\tau_{\max} = 10$ chips for all users, and $K = 10$.

same received power, with E_b/N_0 equal to 20 dB in all simulation studies for output SINRs. Finally, the adaptive implementations of the proposed FBs follow the recursive algorithm provided in [2], with the autocorrelation matrix $\mathbf{R}$ being estimated by the time average $\widehat{\mathbf{R}}(m) = \lambda\widehat{\mathbf{R}}(m-1) + \mathbf{y}(m)\mathbf{y}^H(m)$ with $\lambda = 0.995$.

Convergence of the output SINR has utility in characterizing the performance of an adaptive filter, as $\mathbf{R}$ is estimated by the time average $\widehat{\mathbf{R}}(m)$, to account for time-varying channel statistics. A special feature of the MS filters is that their steady-state output SINRs, as well as their convergence rates, are a function of the number of applied stages. With more stages applied in their reduced-rank implementations, the filters can potentially achieve higher levels of steady-state output SINRs at the cost of slower convergence, due to the fact that larger sample sizes are required to approximate the steady-state reduced-rank autocorrelation matrix $\mathbf{T}_{LD}\mathbf{R}\mathbf{T}_{LD}^H$. As has been shown in Section VI, if the parameter vector Γ_1 of a fading channel is given, then it can be combined with the steering matrix $\mathbf{H}_1$ to form PC MMSE/MOE/BLUE/ML filters. The ranks of the D-stage MRC MMSE/ML FBs can drop from DL to D for PC MMSE/ML filters, and to $D + L - 1$ for PC MOE/BLUE filters. Therefore, a faster convergence rate can potentially be achieved by PC filters. Fig. 5 confirms this conjecture by showing the simulation results of various filters. The convergence of the output SINRs for the six-stage MRC MMSE/MOE/BLUE/ML FBs are presented in this figure, in comparison with the convergence of their PC counterparts of the same number of stages. The spreading gain N is equal to 64, and the spreading sequences are randomly generated for each Monte Carlo run to eliminate the dependence on a specific spreading code. The convergence of the PC filters is obviously faster than that of the MRC FBs. The performance fluctuations at low sample points are due to the fact that the estimate of $\widehat{\mathbf{R}}(m)$ is ill-conditioned for a small number of observations.

The steady-state output SINRs with respect to the number of stages for the reduced-rank MMSE/MOE/BLUE/ML FBs are also studied for both BPSK and DBPSK modulations. The spreading gain $N = 31$ and the spreading sequences are also randomly generated for each Monte Carlo run. The simulation results are evaluated by averaging over 200 Monte Carlo runs. Fig. 6 shows the results of the MRC MMSE/MOE/BLUE/ML FBs for coherent detection of BPSK versus the number of stages. The channel coefficient vector Γ_1 is assumed given, and the maximum allowable delay $\tau_{\max} = 10$ chips. The total rank is equal to DL, and $D = 11$ corresponds to the full-rank implementation $(N = 31)$. It is obvious that the full-rank SINRs can virtually be attained by six-stage reduced-rank implementations.

The output SINRs of the EGC MMSE/MOE/BLUE/ML FBs for noncoherent detection with DBPSK versus the number of stages are shown in Fig. 7. The simulation setup is the same as that for BPSK, except that the soft outputs of the previous symbol serve as the implicit channel estimates of $\Gamma_1 b_1$ in this case. In contrast to the MRC-MMSE-FB, the output SINR of the EGC-MMSE-FB performs the worst among the EGC FBs. The output SINR degrades by 4.6 dB relative to its MRC counterpart, while the output SINR of the EGC-ML-FB degrades by only 1.4 dB relative to the MRC-ML-FB. Due to the fact that the variance of the MMSE estimator of Γ_1 is smaller than that of the BLUE estimator [cf. (42)], an interpretation of this simulation result is that the detection performance in multipath fading channels is more sensitive to the biases of the channel estimates than their variances. The EGC BLUE/ML FBs, both with the unbiased BLUE estimator for $\Gamma_1 b_1$, suffer much less performance degradation than the EGC MMSE/MOE FBs.

To evaluate the impact of delay spreads (or the strength of ISI on the performance of one-shot detection), the sensitivities of the full-rank output SINRs to the maximum allowable delay,

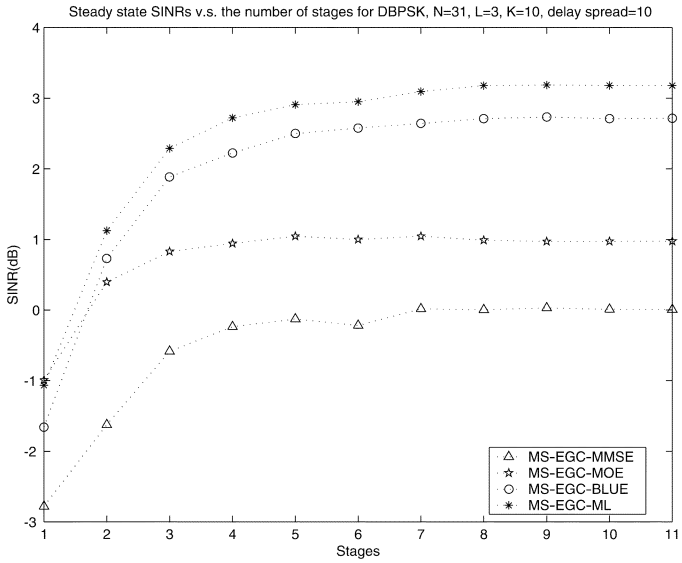

Fig. 7. Steady-state output SINRs of the adaptive reduced-rank EGC MMSE/MOE/BLUE/ML FBs versus the number of stages for DBPSK-modulated signal over a Rayleigh fading channel, with the number of paths $L = 3$, and the normalized Doppler shift $f_d T_s = 5 \times 10^{-3}$. Stage 11 in the plot corresponds to the full-rank $(N = 31)$ SINRs. Maximum allowable delay spread $\tau_{\max} = 10$ chips for all users, and $K = 10$.

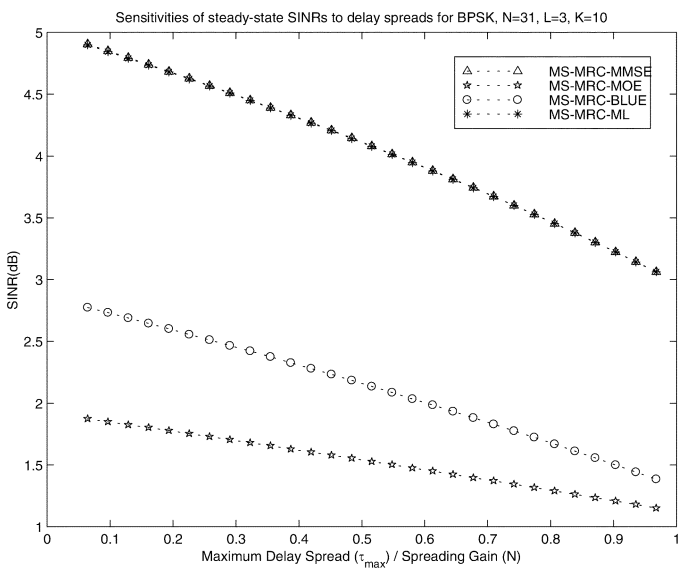

Fig. 8. Steady-state output SINRs of the adaptive full-rank MRC MMSE/MOE/BLUE/ML FBs versus the maximum allowable delay spread for BPSK-modulated signal over a Rayleigh fading channel, with the number of paths $L = 3$, and the normalized Doppler shift $f_d T_s = 5 \times 10^{-3}$. The maximum allowable delay spread $\tau_{\max}$ ranges from 2 to N chips.

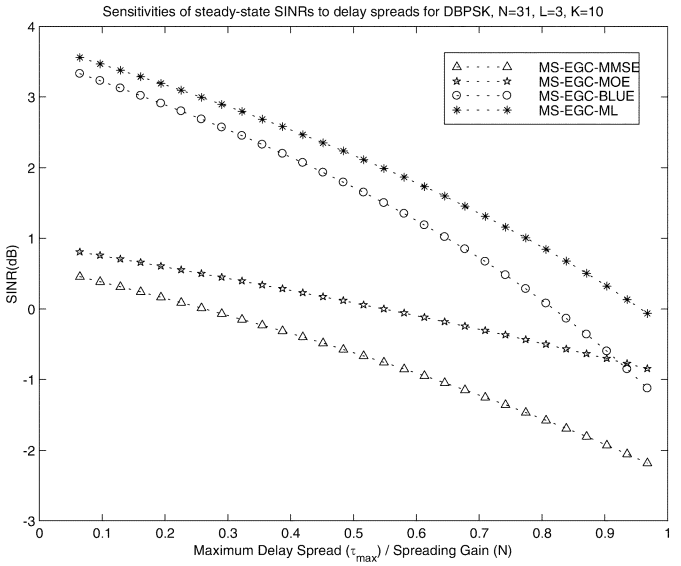

Fig. 9. Steady-state output SINRs of the adaptive full-rank EGC MMSE/MOE/BLUE/ML FBs versus the maximum allowable delay spread for DBPSK-modulated signal over a Rayleigh fading channel with the number of paths $L = 3$, and the normalized Doppler shift $f_d T_s = 5 \times 10^{-3}$. Maximum allowable delay spread $\tau_{\max}$ ranges from 2 to N chips.

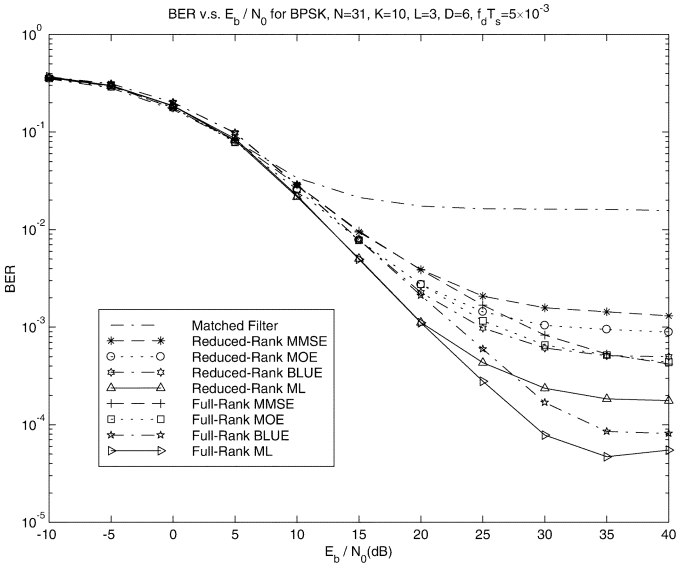

Fig. 10. BER performance of the adaptive reduced-rank MRC MMSE/MOE/BLUE/ML FBs for BPSK-modulated signal over a Rayleigh fading channel with $L = 3$, and the normalized Doppler shift $f_d T_s = 5 \times 10^{-3}$. Maximum allowable delay spread $\tau_{\max} = 5$ chips. Number of stages $D = 6$ for all reduced-rank FBs.

$\tau_{\max}$, are characterized via simulation studies. For each Monte Carlo run of each value of $\tau_{\max}$, the spreading sequences are randomly generated with $N = 31$, and the path delay for each user is also randomly generated for each run. The maximum allowable $\tau_{\max}$ ranges from 2 to 30 chips in simulations. For each value of $\tau_{\max}$, the data is evaluated by averaging over 200 Monte Carlo runs. Fig. 8 shows the results of the full-rank output SINRs for BPSK. The sensitivities of the output SINRs to $\tau_{\max}$ for DBPSK are also presented in Fig. 9. Both results show that MS ML/BLUE FBs are more robust to varying delay spreads. Note that $\tau_{\max}$ has to be greater than $(L-1)T_c$ to maintain the full column-rank assumption for $\mathbf{S}_{1+}$, i.e., rank $\{\mathbf{S}_{1+}\} = L$.

The BER performance for both BPSK/DBPSK-modulated systems are given in Figs. 10 and 11, respectively. Gold codes of length $N = 31$ are adopted in the simulations. For BPSK, the performance of all FBs are comparable. For DBPSK, as implied by the results of the output SINRs, the EGC-ML-FB obviously outperforms other FBs, and the EGC-MMSE-FB is not suggested for noncoherent adaptive detection. It is noted that even though the reduced-rank SINRs are very close to the full-rank ones, full-rank FBs still have BER advantages at high SNR. The

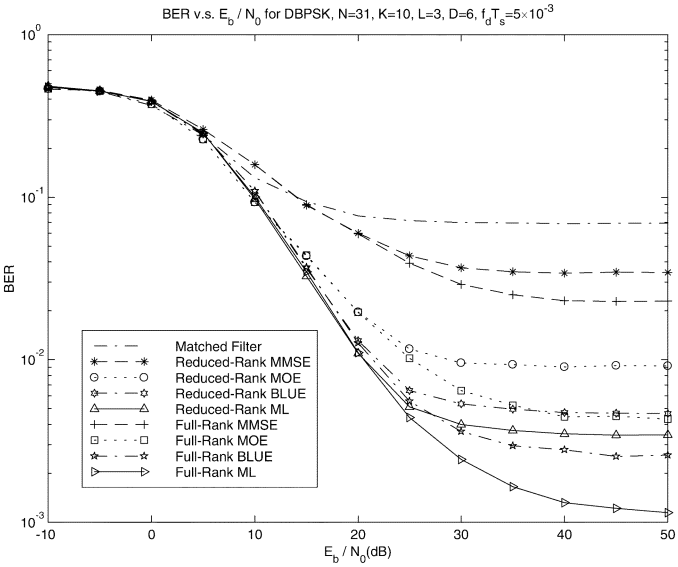

Fig. 11. BER performance of the adaptive reduced-rank EGC MMSE/MOE/BLUE/ML FBs for DBPSK-modulated signal over a Rayleigh fading channel with $L = 3$, and the normalized Doppler shift $f_dT_s = 5 \times 10^{-3}$. Maximum allowable delay spread $\tau_{\max} = 10$ chips. Number of stages $D = 6$ for all reduced-rank FBs.

reason is that even a modest increase in SINR can yield a significant improvement in BER. A complete theoretical performance analysis of the schemes proposed herein can be found in [12] and [13].

VIII. Conclusions

A common structure for MS implementation of reduced-rank MMSE, MOE, ML, and BLUE FBs was developed in this paper. Based on these results, a framework was proposed for joint channel estimation and symbol detection in multipath fading channels. The performance of a family of MRC as well as differential EGC schemes was examined in the context of coherent and noncoherent detection of DS-CDMA in multipath fading channels. Simulation results show that the output SINRs of reduced-rank FBs can attain near full-rank performance with just a few stages. The output SINRs of the PC filters achieve the same performance levels as the MRC FBs with much lower ranks, and thus, faster convergence. Although the output SINRs of the MS MRC MMSE/ML FBs are the highest among the MRC FBs when they serve as symbol detectors, the bias effects of the MMSE/MOE FBs as channel estimators dominate the performance for noncoherent EGC schemes, and thus, cause significant performance degradation. Therefore, the proposed EGC-ML-FB with unbiased BLUE channel estimator exhibits superior performance over the EGC MMSE/MOE FBs proposed in [4] without any additional implementation effort.

Appendix
Proof of *Proposition 1*

Recall that the matched FB of the first stage is given by $E\left(\mathbf{y}\Gamma_1^H b_1^*\right) = \mathbf{S}_{1+}\mathbf{A}_1 = \mathbf{H}_1\mathbf{U}_1$. From Fig. 3, $\mathbf{y}_D = \mathbf{B}_D\mathbf{B}_{D-1}\ldots\mathbf{B}_1\mathbf{y}$. Let blocking matrix $\mathbf{B}_i = \left(\mathbf{I} - \mathbf{H}_i\mathbf{H}_i^H\right)$, $i = 1,\ldots,D$. Then, $\mathbf{y}_D = \prod_{i=D}^{1}\left(\mathbf{I} - \mathbf{H}_i\mathbf{H}_i^H\right)\mathbf{y}$ and $\mathbf{d}_D = \mathbf{H}_D^H\prod_{i=D-1}^{1}\left(\mathbf{I} - \mathbf{H}_i\mathbf{H}_i^H\right)\mathbf{y}$. Moreover, the matched FB $E\left(\mathbf{y}_i\mathbf{d}_i^H\right)$ at each stage i can be decomposed into $\mathbf{H}_i^{N\times L}\mathbf{U}_i^{L\times L}$ by the Gram–Schmidt process. Applying these facts, the proof is achieved by the induction method shown below.

Proof:

1) For stage $i = 2$

$$\begin{aligned}\boldsymbol{\Upsilon}_{\mathbf{y}_1\mathbf{d}_1} &\triangleq E\left(\mathbf{y}_1\mathbf{d}_1^H\right) = \mathbf{B}_1\mathbf{R}\mathbf{H}_1 = \left(\mathbf{I} - \mathbf{H}_1\mathbf{H}_1^H\right)\mathbf{R}\mathbf{H}_1\\ &= \mathbf{H}_2\mathbf{U}_2,\ \mathbf{H}_2^H\mathbf{H}_2 = \mathbf{I}\\ \mathbf{H}_2^H\mathbf{H}_1 &= \mathbf{U}_2^{-H}\mathbf{H}_1^H\mathbf{R}\left(\mathbf{I} - \mathbf{H}_1\mathbf{H}_1^H\right)\mathbf{H}_1 = \mathbf{0}. \end{aligned} \tag{54}$$

Then, we have $\mathbf{H}_1^H\mathbf{H}_1 = \mathbf{I}$, $\mathbf{H}_2^H\mathbf{H}_2 = \mathbf{I}$, and $\mathbf{H}_2 \perp \mathbf{H}_1$.

For stage $i = 3$

$$\begin{aligned}\boldsymbol{\Upsilon}_{\mathbf{y}_2\mathbf{d}_2} &\triangleq E\left(\mathbf{y}_2\mathbf{d}_2^H\right) = \mathbf{B}_2\mathbf{R}_{\mathbf{y}_1}\mathbf{H}_2\\ &= \left(\mathbf{I} - \mathbf{H}_2\mathbf{H}_2^H\right)\left(\mathbf{I} - \mathbf{H}_1\mathbf{H}_1^H\right)\mathbf{R}\left(\mathbf{I} - \mathbf{H}_1\mathbf{H}_1^H\right)\mathbf{H}_2\\ &= \left(\mathbf{I} - \mathbf{H}_2\mathbf{H}_2^H\right)\left(\mathbf{I} - \mathbf{H}_1\mathbf{H}_1^H\right)\mathbf{R}\mathbf{H}_2 = \mathbf{H}_3\mathbf{U}_3\\ \mathbf{H}_3^H\mathbf{H}_3 &= \mathbf{I}\\ \mathbf{H}_3^H\mathbf{H}_i &= \mathbf{U}_3^{-H}\mathbf{H}_2^H\mathbf{R}\left(\mathbf{I} - \mathbf{H}_1\mathbf{H}_1^H\right)\left(\mathbf{I} - \mathbf{H}_2\mathbf{H}_2^H\right)\mathbf{H}_i = \mathbf{0},\\ &\qquad i = 1,2. \end{aligned} \tag{55}$$

Then, we have $\mathbf{H}_i^H\mathbf{H}_i = \mathbf{I}$, $i = 1,\ldots,3$, $\mathbf{H}_3 \perp \mathbf{H}_2$, and $\mathbf{H}_3 \perp \mathbf{H}_1$.

For stage $i = D$, assume $\mathbf{H}_i^H\mathbf{H}_i = \mathbf{I}$, $i = 1,\ldots,D-1$, $\mathbf{H}_{D-1} \perp \mathbf{H}_j$, $j = 1,\ldots,D-2$, and

$$\begin{aligned}\boldsymbol{\Upsilon}_{\mathbf{y}_{D-2}\mathbf{d}_{D-2}} &\triangleq E\left(\mathbf{y}_{D-2}\mathbf{d}_{D-2}^H\right)\\ &= \prod_{j=D-2}^{1}\left(\mathbf{I} - \mathbf{H}_j\mathbf{H}_j^H\right)\mathbf{R}\\ &\quad\times\prod_{j=1}^{D-3}\left(\mathbf{I} - \mathbf{H}_j\mathbf{H}_j^H\right)\mathbf{H}_{D-2}\\ &= \prod_{j=D-2}^{1}\left(\mathbf{I} - \mathbf{H}_j\mathbf{H}_j^H\right)\mathbf{R}\mathbf{H}_{D-2}\\ &= \mathbf{H}_{D-1}\mathbf{U}_{D-1}. \end{aligned} \tag{56}$$

Then, we have

$$\begin{aligned}\boldsymbol{\Upsilon}_{\mathbf{y}_{D-1}\mathbf{d}_{D-1}} &\triangleq E\left(\mathbf{y}_{D-1}\mathbf{d}_{D-1}^H\right)\\ &= \prod_{j=D-1}^{1}\left(\mathbf{I} - \mathbf{H}_j\mathbf{H}_j^H\right)\mathbf{R}\\ &\quad\times\prod_{j=1}^{D-2}\left(\mathbf{I} - \mathbf{H}_j\mathbf{H}_j^H\right)\mathbf{H}_{D-1}\\ &= \prod_{j=D-1}^{1}\left(\mathbf{I} - \mathbf{H}_j\mathbf{H}_j^H\right)\mathbf{R}\mathbf{H}_{D-1} = \mathbf{H}_D\mathbf{U}_D\\ \mathbf{H}_D^H\mathbf{H}_D &= \mathbf{I}\\ \mathbf{H}_D^H\mathbf{H}_l &= \mathbf{U}_D^{-H}\mathbf{H}_{D-1}^H\mathbf{R}\prod_{j=1}^{D-1}\left(\mathbf{I} - \mathbf{H}_j\mathbf{H}_j^H\right)\mathbf{H}_l = \mathbf{0},\\ &\qquad l = 1,\ldots,D-1. \end{aligned} \tag{57}$$

Thus, $\mathbf{H}_i^H\mathbf{H}_i = \mathbf{I}$, $i = 1,\ldots,D$, $\mathbf{H}_D \perp \mathbf{H}_j$, $j = 1,\ldots,D-1$.

By induction, we have $\mathbf{H}_i^H\mathbf{H}_i = \mathbf{I}$ and $\mathbf{H}_i \perp \mathbf{H}_j$, $i \neq j$.

2) From Fig. 3, we see that the received signal $\mathbf{y}$ is multiplied by $\mathbf{H}_i$ and $\mathbf{B}_i$, $i = 1, \ldots, D$, to form the FBs. Therefore, the basis vectors which span the subspace, $\mathcal{T}_{LD}$, for the D-stage FBs are given by the row vectors of the matrix

$$\mathbf{T}_{LD}^H \triangleq \left[\mathbf{H}_1 \mid \mathbf{B}_1\mathbf{H}_2 \mid \cdots \mid \prod_{i=1}^{D-1} \mathbf{B}_i\mathbf{H}_D\right]. \tag{58}$$

Since $\mathbf{H}_i \perp \mathbf{H}_j$, $i \neq j$, we have

$$\prod_{i=1}^{j-1} \mathbf{B}_i\mathbf{H}_j = \prod_{i=1}^{j-1} \left(\mathbf{I} - \mathbf{H}_i\mathbf{H}_i^H\right)\mathbf{H}_j = \mathbf{H}_j, \quad j = 1, \ldots D. \tag{59}$$

Thus

$$\mathbf{T}_{LD}^H = [\mathbf{H}_1 \mid \mathbf{H}_2 \mid \cdots \mid \mathbf{H}_D]. \tag{60}$$

■

REFERENCES

[1] J. S. Goldstein, I. S. Reed, and L. L. Scharf, "A multistage representation of the Wiener filter based on orthogonal projections," *IEEE Trans. Inf. Theory*, vol. 44, pp. 2943–2959, Nov. 1998.

[2] M. L. Honig and J. S. Goldstein, "Adaptive reduced-rank interference suppression based on the multistage Wiener filter," *IEEE Trans. Commun.*, vol. 50, pp. 986–994, Jun. 2002.

[3] M. L. Honig and W. Xiao, "Performance of reduced-rank linear interference suppression," *IEEE Trans. Inf. Theory*, vol. 47, pp. 1928–1946, Jul. 2001.

[4] S. L. Miller, M. L. Honig, and L. B. Milstein, "Performance analysis of MMSE receivers for DS-CDMA in frequency-selective fading channels," *IEEE Trans. Commun.*, vol. 48, pp. 1919–1929, Nov. 2000.

[5] S. Buzzi, M. Lops, and A. M. Tulino, "Partially blind adaptive MMSE interference rejection in asynchronous DS/CDMA networks over frequency-selective fading channels," *IEEE Trans. Commun.*, vol. 49, pp. 94–108, Jan. 2001.

[6] W. Chen and U. Mitra, "Reduced-rank detection schemes for DS-CDMA communication systems," in *Proc. IEEE MILCOM*, vol. 2, 2001, pp. 1065–1069.

[7] U. Madhow and M. L. Honig, "MMSE interference suppression for direct-sequence spread-spectrum CDMA," *IEEE Trans. Commun.*, vol. 42, pp. 3178–3188, Dec. 1994.

[8] M. L. Honig, U. Madhow, and S. Verdú, "Blind adaptive multiuser detection," *IEEE Trans. Inf. Theory*, vol. 41, pp. 944–960, Jul. 1995.

[9] S. M. Kay, *Fundamentals of Statistical Signal Processing: Estimation Theory*. Englewood Cliffs, NJ: Prentice-Hall, 1993.

[10] S. Haykin, *Adaptive Filter Theory*, 3rd ed. Englewood Cliffs, NJ: Prentice-Hall, 1996.

[11] W. Chen, U. Mitra, and P. Schniter, "On the equivalence of three reduced-rank linear estimators with applications to DS-CDMA," *IEEE Trans. Inf. Theory*, vol. 48, pp. 2609–2614, Sep. 2002.

[12] S.-H. Wu, U. Mitra, and C.-C. J. Kuo, "Performance of reduced-rank linear multistage receivers for DS-CDMA in frequency-selective fading channels," *IEEE Trans. Inf. Theory*, submitted for publication.

[13] ——, "Performance analysis of a class of multistage DS-CDMA receivers for multipath channels," in *Proc. IEEE Inf. Theory Workshop*, Paris, France, Apr. 2003, pp. 30–33.

Sau-Hsuan Wu (S'03–M'04) received the B.S. and M.S. degrees in engineering science from National Cheng Kung University, Tainan, Taiwan, R.O.C., in 1990 and 1993, respectively, and the Ph.D. degree in electrical engineering from University of Southern California, Los Angeles, in 2003.

From 1993 to 1995, he served in the Army of Taiwan, and from 1995 to 1999, he was a Circuit and System Design Engineer in Taiwan. Since 2000, he has been with the Department of Electrical Engineering, University of Southern California, first as a Research Assistant and currently as a Postdoctoral Research Fellow. His research interest lies in the application of signal processing theory to communications systems.

Urbashi Mitra (S'88–M'88–SM'04) received the B.S. and M.S. degrees in electrical engineering and computer science from the University of California, Berkeley, in 1987 and 1989, respectively, and the Ph.D. degree in electrical engineering from Princeton University, Princeton, NJ, in 1994.

From 1989 to 1990, she worked as a Member of Technical Staff at Bellcore, Red Bank, NJ. From 1994 to 2000, she was an Assistant Professor in the Department of Electrical Engineering, The Ohio State University (OSU), Columbus. She has been an Associate Professor in the Department of Electrical Engineering, University of Southern California, Los Angeles, since 2000. She has had visiting appointments at the Eurecom Institute, Sophia Antipolis, France; Rice University, Houston, TX; and Stanford University, Stanford, CA.

Dr. Mitra is the recipient of the Texas Instruments Visiting Professor Fellowship, the 2001 Okawa Foundation Award, the 2000 Lumley Award for Research (OSU College of Engineering), the 1997 MacQuigg Award for Teaching (OSU College of Engineering), the 1996 National Science Foundation (NSF) CAREER Award, the 1994 NSF International Postdoctoral Fellowship, the 1998 Lockheed Leadership Fellowship, and the 1987 California Microelectronics Fellowship. She co-chaired the IEEE Communication Theory Symposium at ICC 2003 in Anchorage, AK. She was an Associate Editor for the IEEE TRANSACTIONS ON COMMUNICATIONS from 1996 to 2001. She is currently a Member of the IEEE Information Theory Board of Governors.

C.-C. Jay Kuo (S'83–M'86–SM'92–F'99) received the B.S. degree from National Taiwan University, Taipei, Taiwan, R.O.C., in 1980, and the M.S. and Ph.D. degrees from the Massachusetts Institute of Technology, Cambridge, in 1985 and 1987, respectively, all in electrical engineering.

He was Computational and Applied Mathematics (CAM) Research Assistant Professor in the Department of Mathematics at the University of California, Los Angeles, from October 1987 to December 1988. Since January 1989, he has been with the Department of Electrical Engineering-Systems and the Signal and Image Processing Institute at the University of Southern California, Los Angeles, where he currently has a joint appointment as Professor of Electrical Engineering and Mathematics. His research interests are in the areas of digital signal and image processing, audio and video coding, multimedia communication technologies and delivery protocols, and embedded system design. He is co-author of six books and more than 600 technical publications in international conferences and journals.

Dr. Kuo is a member of SIAM, ACM, and a Fellow of SPIE. He is the Editor-in-Chief for the *Journal of Visual Communication and Image Representation*, Associate Editor for the IEEE TRANSACTIONS ON SPEECH AND AUDIO PROCESSING, and Editor for the *Journal of Information Science and Engineering* and *RURASIP Journal of Applied Signal Processing*. He served as Associate Editor for the IEEE TRANSACTIONS ON IMAGE PROCESSING, 1995–1998, and the IEEE TRANSACTIONS ON CIRCUITS AND SYSTEMS FOR VIDEO TECHNOLOGY, 1995–1997. He received the National Science Foundation Young Investigator Award (NYI) and Presidential Faculty Fellow (PFF) Award in 1992 and 1993, respectively.